The Astrophysical Journal, 784:158 (25pp), 2014 April 1 doi:10.1088/0004-637X/784/2/158

NEUTRON-CAPTURE NUCLEOSYNTHESIS IN THE FIRST STARS*

Ian U. Roederer[1], George W. Preston[2], Ian B. Thompson[2], Stephen A. Shectman[2], and Christopher Sneden[3]
[1] Department of Astronomy, University of Michigan, 500 Church Street, Ann Arbor, MI 48109, USA; iur@umich.edu
[2] Carnegie Observatories, 813 Santa Barbara Street, Pasadena, CA 91101, USA
[3] Department of Astronomy, University of Texas at Austin, 1 University Station C1400, Austin, TX 78712, USA
Received 2013 December 2; accepted 2014 February 17; published 2014 March 18

ABSTRACT

Recent studies suggest that metal-poor stars enhanced in carbon but containing low levels of neutron-capture elements may have been among the first to incorporate the nucleosynthesis products of the first generation of stars. We have observed 16 stars with enhanced carbon or nitrogen using the MIKE Spectrograph on the Magellan Telescopes at Las Campanas Observatory and the Tull Spectrograph on the Smith Telescope at McDonald Observatory. We present radial velocities, stellar parameters, and detailed abundance patterns for these stars. Strontium, yttrium, zirconium, barium, europium, ytterbium, and other heavy elements are detected. In four stars, these heavy elements appear to have originated in some form of *r*-process nucleosynthesis. In one star, a partial *s*-process origin is possible. The origin of the heavy elements in the rest of the sample cannot be determined unambiguously. The presence of elements heavier than the iron group offers further evidence that zero-metallicity rapidly rotating massive stars and pair instability supernovae did not contribute substantial amounts of neutron-capture elements to the regions where the stars in our sample formed. If the carbon- or nitrogen-enhanced metal-poor stars with low levels of neutron-capture elements were enriched by products of zero-metallicity supernovae only, then the presence of these heavy elements indicates that at least one form of neutron-capture reaction operated in some of the first stars.

Key words: nuclear reactions, nucleosynthesis, abundances – stars: abundances – stars: atmospheres – stars: carbon – stars: Population II – stars: Population III

Online-only material: color figures

1. INTRODUCTION

The first stars formed from only the products of big bang nucleosynthesis, yet the metals they produced and distributed into the interstellar medium forever changed the fundamental methods by which molecular gas clouds cool, collapse, and form stars. Cooling by fine structure line emission of ionized carbon (C II), neutral oxygen (O I), and thermal emission from collisionally excited dust grains is suspected to have enabled long-lived low-mass stars to form. Many of the most iron-poor stars known, with Fe/H ratios less than 10^{-4} times the solar ratio, show C/H and O/H ratios of only 10^{-3} to 10^{-1}. This may indicate that substantial enrichment in carbon or oxygen was closely linked with formation of the long-lived low-mass stars that are observable in the solar neighborhood. Theoretical studies of the nucleosynthesis reactions that may have occurred in the first stars have, understandably, focused their effort on production of metals from carbon through the iron group. Elements heavier than the iron group, here considered to be those with $Z > 32$, are difficult to detect observationally in the most iron-poor stars and almost certainly had no effect on subsequent star formation due to their low abundances of 10^{-13} or less per hydrogen atom.

Carbon-enhanced metal-poor stars with no enhancement of neutron-capture elements are commonly referred to as members of the "CEMP-no" class, using the classification scheme proposed by Ryan et al. (2005) and Beers & Christlieb (2005). Ryan et al. proposed that these stars formed from gas clouds pre-enriched with high levels of carbon by previous generations of supernovae, rather than acquiring the carbon enrichment by mass transfer from an evolved companion. The CEMP-no stars include three of the four most iron-poor stars known (Christlieb et al. 2002, 2004; Bessell et al. 2004; Frebel et al. 2005, 2006, 2008; Aoki et al. 2006; Norris et al. 2007, 2012). CEMP-no stars are frequently enhanced in nitrogen (N, $Z = 7$), oxygen (O, $Z = 8$), sodium (Na, $Z = 11$), magnesium (Mg, $Z = 12$), aluminum (Al, $Z = 13$), and silicon (Si, $Z = 14$). A few CEMP-no stars are found in binary systems, but the binary nature of the ensemble of CEMP-no stars is clearly unlike that of the CEMP stars enhanced in material produced by the slow neutron-capture process (the *s*-process) in a companion that passed through the thermally pulsing asymptotic giant branch (TP-AGB) phase of evolution.

Norris et al. (2013) summarize these properties and weigh the evidence that stars in the CEMP-no class were among the first stars to incorporate metals produced by zero-metallicity stars. This evidence includes the chemically primitive stars in ultra-faint dwarf galaxies (e.g., Frebel et al. 2010; Norris et al. 2010a, 2010b; Simon et al. 2010; Koch et al. 2013), including the discovery of a CEMP-no star in each of Segue 1 (Norris et al. 2010a) and Boötes I (Lai et al. 2011; Gilmore et al. 2013); the greater chemical inhomogeneity, on average, of field stars that are kinematically associated with the outer halo (e.g., Fulbright 2002; Stephens & Boesgaard 2002; Gratton et al. 2003; Roederer 2009; Ishigaki et al. 2010, 2013; Nissen & Schuster 2010); the increasing fraction of carbon-enhanced stars with decreasing metallicity and increasing distance above the Galactic plane (Frebel et al. 2006; Carollo et al. 2012); and the low frequency of carbon-enhanced metal-poor damped Lyman-α (DLA) systems at redshifts $2 < z < 6.3$, hinting that an epoch dominated by carbon-enhanced systems, if one existed at all, must have occurred at even higher redshifts (e.g., Cooke

* This paper includes data gathered with the 6.5 m Magellan Telescopes located at Las Campanas Observatory, Chile, and The McDonald Observatory of The University of Texas at Austin.

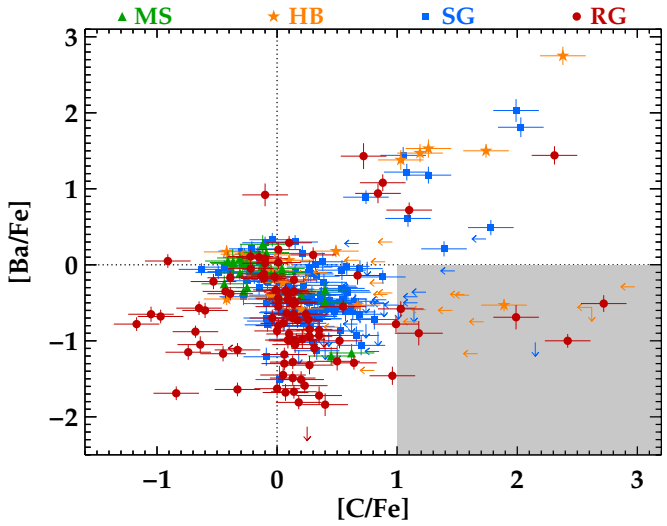

Figure 1. [Ba/Fe] ratios as a function of [C/Fe] ratios for the full sample of stars from Roederer et al. (2014). Green triangles represent unevolved dwarf stars on the main sequence (MS), orange stars represent stars on the horizontal branch (HB), blue squares represent stars beyond the main sequence turn off or on the subgiant branch (SG), and red circles represent stars on the red giant branch (RG). The dotted lines represent the solar ratios. The shaded region marks one criterion for inclusion in our sample, [C/Fe] > +1.0 and [Ba/Fe] < 0.0.

(A color version of this figure is available in the online journal.)

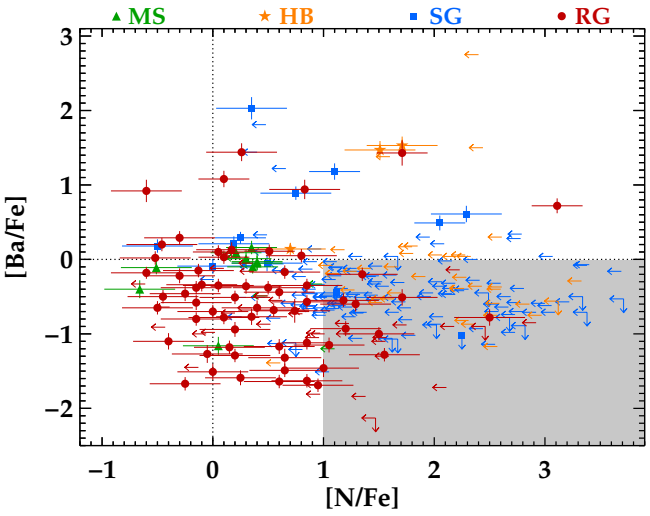

Figure 2. [Ba/Fe] ratios as a function of [N/Fe] ratios for the full sample of stars from Roederer et al. (2014). Symbols are the same as in Figure 1. The shaded region marks one criterion for inclusion in our sample, [N/Fe] > +1.0 and [Ba/Fe] < 0.0.

(A color version of this figure is available in the online journal.)

et al. 2011a, 2011b; Becker et al. 2012; but note that Becker et al. express reservations about the high level of carbon enhancement in the DLA reported by Cooke et al.). These links between carbon enhancement, low metallicity, and remote environments hint that carbon-enhanced stars formed in chemically primitive regions that experienced relatively few enrichment events.

What kind of stars were responsible for prodigious carbon production in the early Universe? The abundance patterns found in the CEMP-no stars are consistent with model predictions for zero-metallicity stars that were massive and rotating (Fryer et al. 2001; Meynet et al. 2006, 2010), underwent faint "mixing and fallback" supernova explosions (Umeda & Nomoto 2003, 2005; Tominaga et al. 2013), or whose supernovae had relativistic jets (Tominaga et al. 2007). These zero-metallicity supernovae are predicted to have seeded pristine gas clouds with carbon, oxygen, and other metals, enabling low-mass star formation to occur.

We now pose a related question: What heavy element ($Z > 32$) abundance patterns are found in stars in the CEMP-no class? We address this question using seven metal-poor stars identified in the abundance survey of Roederer et al. (2014). These stars are carbon-enhanced and barium-poor (Ba, $Z = 56$). We supplement these stars with nine nitrogen-enhanced metal-poor stars that are barium-poor (defined here as NEMP-no; see Johnson et al. 2007) from the same survey. Our goal is not to resolve whether the CEMP-no or NEMP-no stars are the immediate descendants of zero-metallicity stars. Instead, we aim to characterize the heavy element abundance signatures in these stars to motivate studies of neutron-capture nucleosynthesis in stars with zero or extremely low levels of metals. Unfortunately, existing nucleosynthesis calculations for such stars rarely extend to nuclei heavier than the iron group. For example, the reaction network of Tominaga et al. (2013) is truncated at bromine (Br, $Z = 35$), which is several mass units short of the lightest neutron-capture element commonly studied in metal-poor stars, strontium (Sr, $Z = 38$).

Throughout this work, we adopt the standard definitions of elemental abundances and ratios. For element X, the logarithmic abundance is defined as the number of atoms of X per 10^{12} hydrogen atoms, $\log \epsilon(\mathrm{X}) \equiv \log_{10}(N_\mathrm{X}/N_\mathrm{H}) + 12.0$. For elements X and Y, the logarithmic abundance ratio relative to the solar ratio, denoted [X/Y], is defined as $\log_{10}(N_\mathrm{X}/N_\mathrm{Y}) - \log_{10}(N_\mathrm{X}/N_\mathrm{Y})_\odot$. Abundances or ratios denoted with the ionization state indicate the total elemental abundance as derived from transitions of that particular state after ionization corrections have been applied. When reporting relative abundance ratios for elements X and Y, these ratios compare the total abundances of X and Y derived from like ionization states; i.e., neutrals with neutrals and ions with ions.

2. SAMPLE SELECTION

We draw our sample from the catalog of 313 metal-poor stars observed and analyzed by Roederer et al. (2014). Adopting the classification scheme defined by Beers & Christlieb (2005), we identify CEMP or NEMP stars with no enhancement of neutron-capture elements by requiring that a star have [Ba/Fe] < 0.0 and either [C/Fe] > +1.0 or [N/Fe] > +1.0. Figures 1 and 2 illustrate our selection criteria. There are 16 stars with either carbon or nitrogen detection, or both, that lie in the shaded regions. Barium is detected in all but one of these stars (CS 22958–042), and the upper limit on [Ba/Fe] places this star unequivocally in the shaded region. One star is on the horizontal branch (CS 22943–201), two are subgiants (CS 22958–042 and CS 30492–001), and the remaining 13 are red giants. All are field stars and not associated with any known clusters or streams. Our study marks the first detailed abundance study based on high-resolution spectroscopic data for three of these stars (CS 22893–010, CS 22943–201, and CS 30492–001). Many of the remaining 13 stars have been analyzed repeatedly over the last 20 yr by Primas et al. (1994), Thorburn (1994), McWilliam et al. (1995a), Norris et al. (1997, 2001, 2002, 2013), Bonifacio et al. (1998), Giridhar et al. (2001), Preston & Sneden (2001), Aoki et al. (2002a, 2002b, 2002c, 2004), Carretta et al. (2002), Depagne et al. (2002), Cayrel et al. (2004), Spite et al. (2005), Sivarani et al. (2006), François et al. (2007), Cohen et al. (2008,

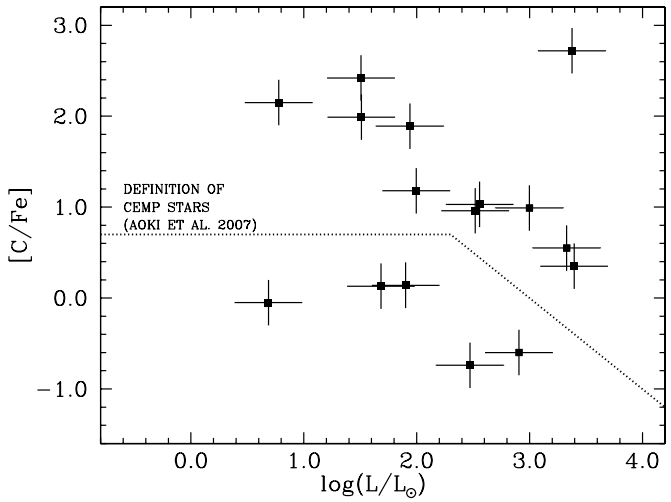

Figure 3. [C/Fe] ratios as a function of luminosity. The squares illustrate the 16 stars in our sample. The dotted line represents the lower bound of the class of CEMP stars as defined by Aoki et al. (2007). The five stars below this line are considered NEMP stars since they all show [N/Fe] > +1.0.

2013), Lai et al. (2008), Ito et al. (2009, 2013), Hollek et al. (2011), Ruchti et al. (2011a), and Yong et al. (2013).

Figure 3 compares the [C/Fe] ratios in our sample with the CEMP definition given by Aoki et al. (2007). Here, we see that 11 stars in our sample would be considered CEMP by their definition. Five stars have low [C/Fe] ratios but show [N/Fe] > +1.0: CS 22878–101, CS 22893–010, CS 22948–066, CS 22960–064, and CS 30492–001. The NEMP stars may or may not be related to the CEMP stars. Including NEMP stars in our sample allows for the possibility that these stars were, at some time in the past, CEMP stars. In this scenario, these stars would have undergone internal mixing, dredging CN-cycled nitrogen-rich and carbon-poor material to the surface. In Section 4.1, we consider whether these NEMP stars constitute a sample distinct from the CEMP stars with regard to their [Fe/H], [Sr/Fe], or [Ba/Fe] ratios.

3. SUMMARY OF OBSERVATIONS AND ANALYSIS TECHNIQUES USED BY ROEDERER ET AL. (2014)

This section summarizes the observations and analysis techniques used by Roederer et al. (2014) to measure radial velocities, derive stellar parameters, and derive abundances. All of the values discussed here are presented in the tables in that work. Several of those tables are only available online, so we feel it is helpful to reproduce this information here for the 16 CEMP-no and NEMP-no stars for easy reference.

3.1. Observations

Most observations were made with the Magellan Inamori Kyocera Echelle (MIKE) spectrograph (Bernstein et al. 2003) on the 6.5 m Walter Baade and Landon Clay Telescopes at Las Campanas Observatory. These spectra were taken with the $0\farcs7 \times 5\farcs0$ slit, yielding a resolving power of $R \equiv \lambda/\Delta\lambda \sim 41{,}000$ in the blue and $R \sim 35{,}000$ in the red as measured from isolated ThAr lines in the comparison lamp images. A dichroic splits the two arms at ≈4950 Å. This setup achieves complete wavelength coverage from 3350 to 9150 Å. Data reduction, extraction, sky subtraction, and wavelength calibration were performed using the MIKE data reduction pipeline written by Dan Kelson (see Kelson 2003).

Observations of BD+44 493 were made with the Robert G. Tull Coudé Spectrograph (Tull et al. 1995) on the 2.7 m Harlan J. Smith Telescope at McDonald Observatory. These spectra were taken with the $2\farcs4 \times 8\farcs0$ slit, yielding a resolving power $R \sim 33{,}000$. This setup delivers complete wavelength coverage from 3700–5700 Å, with small gaps between the echelle orders further to the red. For our analysis we only use the spectra blueward of 8000 Å. Data reduction, extraction, sky subtraction, and wavelength calibration were performed using the REDUCE software package (Piskunov & Valenti 2002). Coaddition and continuum normalization for both sets of spectra were performed within the IRAF environment.

Table 1 presents a record of observations. Signal-to-noise (S/N) estimates, listed in Table 2, are based on Poisson statistics of the photons collected in the continuum at several reference wavelengths.

3.2. Radial Velocity Measurements

Roederer et al. (2014) measured radial velocities by cross-correlating the spectral order containing the Mg I b lines against metal-poor template standards. Heliocentric corrections were computed using the IRAF *rvcorrect* task. Table 1 lists the heliocentric velocity measurements for each observation. Typical uncertainties are ≈0.6–0.8 km s^{-1} per observation.

BD+44 493, CS 22891–200, CS 22943–201, CS 22948–066, CS 22949–037, CS 29498–043, CS 29502–092, and CS 30314–067 are consistent with no velocity variations at the ≈2 km s^{-1} level. This conclusion is based on comparisons with velocity measurements by other investigators (Primas et al. 1994; McWilliam et al. 1995b; Aoki et al. 2002a, 2002b; Norris et al. 2001; Cohen et al. 2002, 2008, 2013; Depagne et al. 2002; Carney et al. 2003; Lai et al. 2004; Bonifacio et al. 2009; Hollek et al. 2011; Ito et al. 2013) or repeat observations separated by more than two months.

CS 22877–001 exhibits radial velocity variations at a full amplitude of ≈4 km s^{-1} (Giridhar et al. 2001; Aoki et al. 2002a; Tsangarides et al. 2004). Our own measurements span a range of 3.2 km s^{-1} over 3.5 yr.

Radial velocity measurements of CS 22878–101 have been reported by several authors, including McWilliam et al. (1995a), Cohen et al. (2002), Lai et al. (2004), and Bonifacio et al. (2009). These measurements span a range of 3 km s^{-1} and may be expected to have internal precisions of better than 1 km s^{-1}, though it is difficult to assess the systematic uncertainty from one author to another. CS 22878–101 may exhibit low-amplitude radial velocity variations.

Our measured velocity of CS 22893–010 is 24 km s^{-1} different than that measured from a medium-resolution spectrum obtained by Lai et al. (2004). They report a measurement uncertainty of 4.2 km s^{-1}. It seems probable that CS 22893–010 exhibits radial velocity variations, but no other radial velocity information is available for this star.

Variations in the velocity of CS 22957–027 have been confirmed by Preston & Sneden (2001), who supplemented their own observations with measurements by Norris et al. (1997) and Bonifacio et al. (1998). Subsequent observations through 2012 May, by G. Preston (to be published elsewhere) reveal that the original orbital period reported by Preston & Sneden is an alias; the current best-fit orbit has a period of ≈1078 days and a systemic velocity of −67.7 km s^{-1}.

Sivarani et al. (2006) reported radial velocity variations in CS 22958–042 among their observations that spanned less than 1 hr. Our radial velocity measurements, spanning 3 days, are

Table 1
Log of Observations

Star	Telescope/ Instrument	Exposure Length (s)	Date	UT at Mid-exposure	Heliocentric Julian Date	Heliocentric Radial Velocity (km s^{-1})
BD+44 493	McDonald-Smith/Tull	7200	2008 Aug 14	10:56	2454692.956	−149.7
BD+44 493	McDonald-Smith/Tull	3600	2008 Nov 04	09:01	2454774.881	−150.0
CS 22877–001	Magellan-Baade/MIKE	1000	2003 Jan 14	06:58	2452653.790	+169.8
CS 22877–001	Magellan-Baade/MIKE	1600	2003 Jan 15	07:52	2452654.828	+167.0
CS 22877–001	Magellan-Baade/MIKE	1200	2003 Jan 20	08:31	2452659.856	+166.6
CS 22877–001	Magellan-Clay/MIKE	1800	2006 Aug 02	23:07	2453950.461	+166.7
CS 22878–101	Magellan-Clay/MIKE	2400	2006 Aug 05	23:59	2453953.501	−128.8
CS 22891–200	Magellan-Clay/MIKE	4100	2006 Aug 06	01:05	2453953.549	+137.2
CS 22893–010	Magellan-Clay/MIKE	3600	2012 Aug 27	02:48	2456166.622	−51.6
CS 22943–201	Magellan-Clay/MIKE	2200	2005 Aug 21	01:26	2453603.564	+37.2
CS 22943–201	Magellan-Clay/MIKE	5100	2006 Jun 12	05:54	2453898.750	+37.6
CS 22943–201	Magellan-Clay/MIKE	1500	2007 Aug 03	06:22	2454315.771	+35.4
CS 22943–201	Magellan-Clay/MIKE	1800	2007 Aug 04	04:04	2454316.675	+36.4
CS 22948–066	Magellan-Clay/MIKE	1500	2007 Aug 22	02:48	2454334.622	−171.2
CS 22948–066	Magellan-Clay/MIKE	900	2009 May 15	10:32	2454966.940	−170.8
CS 22949–037	Magellan-Clay/MIKE	5000	2006 Aug 06	08:32	2453953.860	−125.4
CS 22949–037	Magellan-Clay/MIKE	1350	2009 Jul 25	08:04	2455037.840	−125.3
CS 22957–027	Magellan-Clay/MIKE	1000	2008 Sep 11	06:13	2454720.765	−74.8
CS 22958–042	Magellan-Baade/MIKE	4800	2003 Jan 16	01:30	2452655.561	+165.2
CS 22958–042	Magellan-Baade/MIKE	2400	2003 Jan 17	01:10	2452656.547	+165.7
CS 22958–042	Magellan-Baade/MIKE	2400	2003 Jan 19	01:14	2452658.550	+165.6
CS 22960–064	Magellan-Clay/MIKE	3000	2006 Jul 22	06:58	2453938.795	−86.4
CS 29498–043	Magellan-Clay/MIKE	6000	2013 Apr 22	08:54	2456404.870	−32.3
CS 29498–043	Magellan-Clay/MIKE	3300	2013 Apr 23	09:20	2456405.888	−32.3
CS 29502–092	Magellan-Clay/MIKE	1800	2009 Oct 26	01:32	2455130.567	−66.6
CS 30314–067	Magellan-Clay/MIKE	1800	2013 Apr 21	09:34	2456403.898	+145.6
CS 30492–001	Magellan-Clay/MIKE	1650	2008 Sep 10	01:18	2454719.558	−116.2
HE 1012−1540	Magellan-Clay/MIKE	1800	2013 Apr 21	23:40	2456404.489	+225.4
HE 1012−1540	Magellan-Clay/MIKE	5400	2013 Apr 23	01:45	2456405.576	+225.8

Table 2
Observational Stellar Data

Star	Total Exp. Time (s)	No. Obs.	S/N 3950 Å	S/N 4550 Å	S/N 5200 Å	S/N 6750 Å
BD+44 493	10800	2	85	170	220	285
CS 22877–001	5600	4	150	230	265	405
CS 22878–101	2400	1	60	95	75	115
CS 22891–200	4100	1	65	105	85	130
CS 22893–010	3600	1	45	75	65	115
CS 22943–201	10600	4	85	120	85	120
CS 22948–066[a]	2400	2	60	95	80	130
CS 22949–037[b]	6350	2	65	100	85	135
CS 22957–027[c]	1000	1	40	55	60	95
CS 22958–042	9600	3	60	90	110	155
CS 22960–064	3000	1	75	110	80	110
CS 29498–043	9300	2	70	140	135	280
CS 29502–092	1800	1	50	85	90	165
CS 30314–067	1800	1	85	165	165	350
CS 30492–001	1650	1	55	75	70	115
HE 1012−1540	7200	2	60	95	85	150

Notes.
[a] CS 30343–064.
[b] HE 2323−0256.
[c] HE 2356−0410.

consistent with a single value and fall within the range of their observations.

Cohen et al. (2008) report a 4σ difference in their two radial velocity measurements of HE 1012−1540, although these measurements taken 3 yr apart are different by only 1.5 km s^{-1}. One subsequent observation of this star 10 yr later by Cohen et al. (2013) expands the range to 1.9 km s^{-1}. Our radial velocity measurements are separated by only 1 day, but they agree with each other and fall within the range reported by Cohen et al.

We are aware of only our single epoch radial velocities measured from high-resolution spectroscopic observations for CS 22960–064 and CS 30492–001.

In summary, 8 of the 16 stars in our sample show no evidence for radial velocity variations. A binary orbital solution has been determined previously for one star. Another shows tentative evidence for large-amplitude velocity variations. Four stars show evidence of low-amplitude velocity variations. Two stars have only been observed at high spectral resolution at a single epoch. Follow-up velocity observations of CS 22877–001, CS 22878–101, CS 22893–010, CS 22958–042, CS 22960–064, CS 30492–001, and HE 1012−1540 would be of interest.

3.3. Equivalent Width Measurements

Roederer et al. (2014) measured equivalent widths using a semi-automatic routine that fits Voigt absorption line profiles to continuum-normalized spectra. Comparison with equivalent widths measured by Johnson (2002), Cayrel et al. (2004), Honda et al. (2004), and Lai et al. (2008) indicates that the standard deviation of the residuals is 3.5 mÅ for 3087 lines with equivalent width <100 mÅ.

3.4. Model Atmospheres

Roederer et al. (2014) used model atmospheres interpolated from the grid of one-dimensional MARCS models (Gustafsson et al. 2008) and performed the analysis using the latest version

Table 3
Magnitudes and Atmospheric Parameters

Star	V	$T_{\rm eff}$ (K)	log g	v_t (km s^{-1})	[M/H][a]
BD+44 493	9.11	5040 (36)	2.10 (0.14)	1.35 (0.06)	−4.26 (0.03)
CS 22877–001	12.16	4790 (34)	1.45 (0.14)	1.55 (0.06)	−3.24 (0.06)
CS 22878–101	13.73	4650 (35)	1.05 (0.14)	1.90 (0.06)	−3.30 (0.06)
CS 22891–200	13.93	4490 (33)	0.50 (0.12)	1.70 (0.06)	−3.88 (0.08)
CS 22893–010	14.74	5150 (44)	2.45 (0.20)	1.35 (0.06)	−2.93 (0.07)
CS 22943–201	15.98	5970 (52)	2.45 (0.39)	1.60 (0.06)	−2.69 (0.06)
CS 22948–066	13.47	4830 (34)	1.55 (0.15)	2.00 (0.06)	−3.18 (0.07)
CS 22949–037	14.36	4630 (34)	0.95 (0.13)	1.70 (0.06)	−4.21 (0.05)
CS 22957–027	13.60	5220 (39)	2.65 (0.23)	1.45 (0.06)	−3.00 (0.07)
CS 22958–042	14.52	5760 (57)	3.55 (0.18)	0.95 (0.08)	−2.99 (0.15)
CS 22960–064	13.94	5060 (36)	2.20 (0.14)	1.40 (0.06)	−2.77 (0.07)
CS 29498–043	13.72	4440 (20)	0.50 (0.13)	1.75 (0.06)	−3.85 (0.08)
CS 29502–092	11.87	4820 (34)	1.50 (0.14)	1.50 (0.06)	−3.20 (0.07)
CS 30314–067	11.85	4320 (12)	0.50 (0.10)	1.85 (0.06)	−3.01 (0.06)
CS 30492–001	14.20	5790 (50)	3.65 (0.15)	0.85 (0.07)	−2.35 (0.07)
HE 1012−1540	14.04	5230 (32)	2.65 (0.20)	1.70 (0.06)	−3.76 (0.14)

Note. [a] [M/H] is adopted to equal [Fe/H] as derived from Fe II lines.

of the spectral line analysis code MOOG (Sneden 1973; see also Sobeck et al. 2011). The stars in our sample show strong absorption from molecular bands, so it is advisable to avoid deriving the model atmosphere parameters from color–temperature relations based on broadband photometry. Instead, effective temperatures ($T_{\rm eff}$) were derived by requiring that abundances derived from Fe I lines showed no trend with the excitation potential of the lower level of the transition. Microturbulent velocities (v_t) were derived by requiring that abundances derived from Fe I lines showed no trend with line strength. Surface gravities (log g, in cgs units) were calculated from the relationship between $T_{\rm eff}$ and log g given by theoretical isochrones in the Y^2 grid (Demarque et al. 2004); an age of 12 ± 1.5 Gyr was assumed for all stars. The iron abundance derived from Fe II lines was taken to represent the overall metallicity, [M/H]. This method was used for the 15 stars not on the horizontal branch. For the one star on the horizontal branch, log g was derived by requiring that the iron abundance derived from neutral iron lines matches that derived from ionized iron lines. The derived model parameters and their statistical (internal) uncertainties are presented in Table 3.

To evaluate the reliability of the model atmosphere parameters derived for the full sample, Roederer et al. (2014) compared these values with parameters derived by a variety of different methods for stars in common with previous studies. For red giants, subgiants, and stars on the horizontal branch, these comparisons for the full sample yielded standard deviations of 151, 211, and 156 K in $T_{\rm eff}$, 0.40, 0.34, and 0.42 in log g, 0.41, 0.33, and 0.26 km s^{-1} in v_t, and 0.24, 0.22, and 0.16 dex in [Fe II/H]. We adopt these as the systematic uncertainties in the model atmosphere parameters.

Table 4 compares the derived $T_{\rm eff}$ and metallicity with those found by previous investigators for the CEMP-no and NEMP-no stars in our sample. Most of these previous studies calculated $T_{\rm eff}$ using color–$T_{\rm eff}$ relations, frequently leading to warmer $T_{\rm eff}$ and higher metallicity for the red giants. Even so, there is a fair amount of scatter in the derived values, and Table 4 shows that our values are reasonable given the different methods employed. Roederer et al. (2014) found that the derived metallicities were, on average, lower than those found by previous studies by 0.25, 0.04, and 0.12 dex for red giants (108 stars), subgiants (40 stars), and stars on the horizontal branch (28 stars), respectively. For

Table 4
Comparison of Derived Model Parameters with Previous Work

Star	$T_{\rm eff}$	log g	[Fe/H][a]	Reference
BD+44 493	5040	2.10	−4.26	This study
	5510	3.70	−3.68	Ito et al. (2009)
	5430	3.40	−3.82	Ito et al. (2013)
CS 22877–001	4790	1.45	−3.24	This study
	5000	1.50	−2.88	Giridhar et al. (2001)
	5100	2.20	−2.71	Aoki et al. (2002a)
CS 22878–101	4650	1.50	−3.30	This study
	4790	1.15	−3.13	McWilliam et al. (1995a)
	4775	1.30	−3.13	Carretta et al. (2002)
	4800	1.30	−3.21	Cayrel et al. (2004)
	4789	1.72	−3.00	Lai et al. (2004)
	4730	1.30	−3.27	Cohen et al. (2013)
CS 22891–200	4490	0.50	−3.88	This study
	4700	0.45	−3.48	McWilliam et al. (1995a)
	4500	1.00	−3.92	Hollek et al. (2011)
CS 22893–010	5150	2.45	−2.93	This study
	5528	3.44	−2.50	Lai et al. (2004)
CS 22948–066	4830	1.55	−3.18	This study
	5170	1.80	−3.16	Primas et al. (1994)
	5020	1.45	−3.04	McWilliam et al. (1995a)
	5100	1.80	−3.14	Cayrel et al. (2004)
CS 22949–037	4630	0.95	−4.21	This study
	4810	2.10	−3.99	McWilliam et al. (1995a)
	4900	1.70	−3.79	Norris et al. (2001)
	4900	1.50	−3.94	Depagne et al. (2002)
	4915	1.70	−3.73	Cohen et al. (2008)
	4915	1.70	−3.93	Cohen et al. (2013)
CS 22957–027	5220	2.65	−3.00	This study
	4850	1.90	−3.38	Norris et al. (1997)
	4839	2.25	−3.43	Bonifacio et al. (1998)
	5050	2.00	−2.96	Preston & Sneden (2001)
	5100	1.90	−3.11	Aoki et al. (2002b)
	5205	2.50	−3.13	Cohen et al. (2006)
CS 22958–042	5760	3.55	−2.99	This study
	6217	3.50	−3.34	Thorburn (1994)
	6250	3.50	−2.93	Sivarani et al. (2006)
CS 29498–043	4440	0.50	−3.85	This study
	4400	0.60	−3.75	Aoki et al. (2002b)
	4600	1.20	−3.53	Aoki et al. (2004)
	4639	1.00	−3.49	Yong et al. (2013)
CS 29502–092	4820	1.50	−3.20	This study
	5000	2.10	−2.76	Aoki et al. (2002a)
	5114	2.51	−3.00	Lai et al. (2004)
	4890	1.72	−3.20	Lai et al. (2008)
	5123	2.20	−2.83	Ruchti et al. (2011a)
CS 30314–067	4320	0.50	−3.01	This study
	4400	0.70	−2.85	Aoki et al. (2002a)
HE 1012−1540	5230	2.65	−3.76	This study
	5620	3.40	−3.71	Cohen et al. (2008)
	5745	3.45	−3.47	Yong et al. (2013)

Note. [a] As derived from Fe II lines, if specified.

the 13 stars listed in Table 4, our metallicities are lower than those found by previous studies by 0.17 dex ($\sigma = 0.25$).

3.5. Abundance Analysis

Table 8 of Roederer et al. (2014) lists the line wavelength, species identification, excitation potential of the lower level, and log gf value for each transition examined. Spectrum synthesis matching was performed for lines broadened by hyperfine splitting or in cases where a significant isotope shift may be present. Damping constants were adopted from Barklem

et al. (2000) and Barklem & Aspelund-Johansson (2005) when available, otherwise the standard Unsöld (1955) approximation was used. Line lists were generated using the Kurucz & Bell (1995) lists and updated using more recent experimental data when available. For unblended lines, Roederer et al. used MOOG to compute theoretical equivalent widths, which were then forced to match measured equivalent widths by adjusting the abundance. When a line was not detected, Roederer et al. derived 3σ upper limits on the abundance. Table 11 of Roederer et al. lists the abundances derived from each line in each star. Relative abundances were computed with respect to the solar ratios given by Asplund et al. (2009) and are listed in Table 13 of Roederer et al.

Carbon abundances were derived from the CH $A^2\Delta - X^2\Pi$ G band. The C_2 $d^3\Pi - a^3\Pi$ (0, 0) Swan bands were detected in three stars, CS 22957–027, CS 22958–042, and CS 29498–043. The carbon abundances derived from the CH and C_2 bands only agree within a factor of $\approx$3 with a fair amount of scatter, and we will continue to investigate these discrepancies elsewhere. Nitrogen abundances were derived from the NH $A^3\Pi - X^3\Sigma$ band, if detected. The CN $B^2\Sigma - X^2\Sigma$ band was also detected in seven stars in our sample. Nitrogen abundances derived from these bands show a consistent offset of 0.32 ± 0.10 dex with the nitrogen abundance derived from CN being higher. Since NH was detected more frequently than CN, we adopt the nitrogen abundances derived from NH unless the S/N at the NH band was too low to enable a measurement or upper limit.

Roederer et al. (2014) leveraged their large data set to identify lines yielding derived abundances systematically lower or higher than other lines of the same species. This effort minimized systematic effects resulting from using different lines as abundance indicators. A list of these corrections is given in Table 16 of Roederer et al. Independently, that study also adopted corrections to account for departures from local thermodynamic equilibrium (LTE) in the line formation regions for Li I (Lind et al. 2009), O I (Fabbian et al. 2009), Na I (Lind et al. 2011), and K I (Takeda et al. 2002). These corrections are listed in Table 15 of Roederer et al.

Weighted mean abundances and uncertainties were computed using the formalism presented in McWilliam et al. (1995a), as discussed in detail in Roederer et al. (2014). These abundances are reported for each CEMP-no and NEMP-no star in Tables 5–20. Several sets of uncertainties are listed in each table. The statistical uncertainty, $\sigma_{\rm statistical}$, accounts for uncertainties in the equivalent widths, $\log gf$ values, non-LTE corrections, and line-by-line offset corrections. The total uncertainty, $\sigma_{\rm total}$, accounts for the statistical uncertainty and uncertainties in the model atmosphere parameters. The other two uncertainties listed in Tables 5–20 are approximations to the abundance ratio uncertainties given by Equations (A19) and (A20) of McWilliam et al. The quantity $\sigma_{\rm neutrals}$ for element A should be added in quadrature with $\sigma_{\rm statistical}$ for element B when computing the ratio [A/B] when B is derived from neutral lines. Similarly, $\sigma_{\rm ions}$ for element A should be added in quadrature with $\sigma_{\rm statistical}$ for element B when element B is derived from ionized lines.

We examine the $^{12}C/^{13}C$ isotope ratio in each star in our sample using seven isolated CH features between 4209 and 4222 Å. (Roederer et al. 2014 did not measure the $^{12}C/^{13}C$ ratios for any stars in their sample.) Six stars yielded only lower limits on $^{12}C/^{13}C$, and in three stars the CH features were too weak to estimate this ratio reliably. ^{13}CH features are identified in the other seven stars. These results are listed in Table 21.

Table 5
Mean Abundances in BD+44 493

Species	$N_{\rm lines}$	$\log\epsilon$	[X/Fe][a]	$\sigma_{\rm statistical}$	$\sigma_{\rm total}$	$\sigma_{\rm neutrals}$	$\sigma_{\rm ions}$
Fe I	61	3.22	−4.28	0.09	0.16	0.00	0.00
Fe II	2	3.24	−4.26	0.12	0.18	0.00	0.00
Li I	1	0.64	...	0.12	0.18	0.15	0.23
C (CH)	1	5.35	1.18	0.15	0.25	0.20	0.22
N (CN)	1	<5.75	<2.18	...	...	...	...
O I	0	...	...	...	...	...	...
Na I	0	...	...	...	...	...	...
Mg I	7	4.21	0.90	0.09	0.16	0.12	0.22
Al I	1	1.73	−0.44	0.09	0.16	0.12	0.22
Si I	1	3.71	0.48	0.16	0.28	0.24	0.32
K I	0	...	...	...	...	...	...
Ca I	6	2.57	0.52	0.15	0.20	0.17	0.25
Sc II	1	−1.06	0.05	0.05	0.15	0.19	0.13
Ti I	3	0.90	0.24	0.19	0.23	0.21	0.27
Ti II	9	0.68	−0.02	0.08	0.16	0.19	0.15
V I	0	...	...	...	...	...	...
V II	2	<0.31	<0.64	...	...	...	...
Cr I	2	1.04	−0.31	0.10	0.17	0.14	0.22
Cr II	0	...	...	...	...	...	...
Mn I	2	0.10	−1.05	0.16	0.20	0.18	0.25
Mn II	0	...	...	...	...	...	...
Co I	3	1.00	0.29	0.15	0.20	0.17	0.25
Ni I	2	2.08	0.14	0.14	0.19	0.16	0.24
Cu I	0	...	...	...	...	...	...
Zn I	2	<1.39	<1.11	...	...	...	...
Ga I	1	<0.35	<1.59	...	...	...	...
Rb I	0	...	...	...	...	...	...
Sr II	2	−1.96	−0.58	0.05	0.15	0.18	0.13
Y II	6	<−2.49	<−0.44	...	...	...	...
Zr II	3	<−1.02	<0.66	...	...	...	...
Nb II	1	<0.34	<3.14	...	...	...	...
Mo I	1	<−0.47	<1.93	...	...	...	...
Tc I	1	<0.03	...	...	...	...	...
Ru I	0	...	...	...	...	...	...
Sn I	0	...	...	...	...	...	...
Ba II	1	−2.98	−0.90	0.10	0.17	0.21	0.16
La II	0	...	...	...	...	...	...
Ce II	5	<−1.66	<1.02	...	...	...	...
Pr II	4	<−2.00	<1.54	...	...	...	...
Nd II	5	<−1.82	<1.02	...	...	...	...
Sm II	2	<−1.60	<1.70	...	...	...	...
Eu II	4	<−2.83	<0.91	...	...	...	...
Gd II	2	<−1.31	<1.88	...	...	...	...
Tb II	3	<−1.82	<2.14	...	...	...	...
Dy II	3	<−2.01	<1.15	...	...	...	...
Ho II	2	<−2.21	<1.57	...	...	...	...
Er II	3	<−1.74	<1.60	...	...	...	...
Tm II	2	<−2.16	<2.00	...	...	...	...
Yb II	1	<−2.40	<0.94	...	...	...	...
Hf II	2	<−1.08	<2.33	...	...	...	...
Ir I	0	...	...	...	...	...	...
Pb I	1	<0.38	<2.62	...	...	...	...
Th II	2	<−1.89	<2.31	...	...	...	...

Note. [a] [Fe/H] is indicated for Fe I and Fe II.

4. RESULTS

4.1. Iron, Strontium, and Barium

Figure 4 shows the metallicity distribution of our sample, which spans a range of $-4.3 <$ [Fe/H] < -2.3; the median [Fe/H] is −3.2. (Recall that our metallicities are $\approx$0.17 dex lower than those found by previous studies that derived $T_{\rm eff}$ by different methods; see Section 3.4.) The metallicities of our

Table 6
Mean Abundances in CS 22877–001

Species	N_{lines}	$\log \epsilon$	[X/Fe][a]	$\sigma_{statistical}$	σ_{total}	$\sigma_{neutrals}$	σ_{ions}
Fe I	106	4.19	−3.31	0.06	0.15	0.00	0.00
Fe II	10	4.26	−3.24	0.07	0.15	0.00	0.00
Li I	1	0.66	...	0.09	0.16	0.11	0.19
C (CH)	1	6.22	1.03	0.15	0.25	0.19	0.19
N (NH)	1	4.44	−0.15	0.30	0.36	0.32	0.32
O I	2	6.60	1.21	0.18	0.22	0.19	0.25
Na I	0	...	...	...	...	...	...
Mg I	8	4.67	0.38	0.05	0.16	0.09	0.18
Al I	1	2.41	−0.73	0.09	0.29	0.23	0.29
Si I	0	...	...	...	...	...	...
K I	0	...	...	...	...	...	...
Ca I	9	3.41	0.37	0.11	0.17	0.13	0.20
Sc II	5	−0.33	−0.24	0.07	0.15	0.18	0.10
Ti I	15	1.71	0.06	0.08	0.15	0.10	0.19
Ti II	25	1.78	0.07	0.07	0.15	0.18	0.10
V I	0	...	...	...	...	...	...
V II	2	0.53	−0.17	0.25	0.29	0.30	0.26
Cr I	10	2.12	−0.22	0.08	0.16	0.10	0.19
Cr II	3	2.45	0.05	0.12	0.18	0.20	0.14
Mn I	2	1.67	−0.45	0.08	0.16	0.11	0.19
Mn II	4	1.63	−0.57	0.16	0.21	0.23	0.17
Co I	7	1.58	−0.10	0.14	0.21	0.16	0.23
Ni I	7	2.85	−0.07	0.12	0.22	0.16	0.23
Cu I	0	...	...	...	...	...	...
Zn I	2	1.48	0.22	0.12	0.18	0.14	0.21
Ga I	0	...	...	...	...	...	...
Rb I	1	<1.90	<2.69	...	...	...	...
Sr II	2	−0.60	−0.23	0.04	0.25	0.25	0.26
Y II	2	−1.58	−0.55	0.12	0.18	0.21	0.14
Zr II	3	−0.78	−0.13	0.12	0.18	0.21	0.14
Nb II	1	<−0.24	<1.54	...	...	...	...
Mo I	1	<−0.68	<0.75	...	...	...	...
Tc I	1	<0.22	...	...	...	...	...
Ru I	0	...	...	...	...	...	...
Sn I	1	<0.77	<2.01	...	...	...	...
Ba II	2	−1.63	−0.58	0.05	0.15	0.17	0.10
La II	2	−2.23	−0.09	0.18	0.23	0.25	0.19
Ce II	1	<−0.95	<0.71	...	...	...	...
Pr II	2	<−2.40	<0.12	...	...	...	...
Nd II	1	−1.94	−0.12	0.12	0.18	0.21	0.14
Sm II	1	<−1.78	<0.50	...	...	...	...
Eu II	2	−2.76	−0.05	0.13	0.19	0.21	0.15
Gd II	2	<−1.30	<0.87	...	...	...	...
Tb II	3	<−2.14	<0.80	...	...	...	...
Dy II	2	−1.99	0.15	0.19	0.23	0.25	0.20
Ho II	0	...	...	...	...	...	...
Er II	1	−2.10	0.22	0.29	0.33	0.34	0.30
Tm II	2	<−2.36	<0.78	...	...	...	...
Yb II	1	−2.55	−0.23	0.19	0.23	0.25	0.20
Hf II	2	<−1.27	<1.12	...	...	...	...
Ir I	1	<−0.75	<1.18	...	...	...	...
Pb I	1	<0.40	<1.67	...	...	...	...
Th II	0	...	...	...	...	...	...

Note. [a] [Fe/H] is indicated for Fe I and Fe II.

Table 7
Mean Abundances in CS 22878–101

Species	N_{lines}	$\log \epsilon$	[X/Fe][a]	$\sigma_{statistical}$	σ_{total}	$\sigma_{neutrals}$	σ_{ions}
Fe I	100	3.97	−3.53	0.06	0.15	0.00	0.00
Fe II	11	4.20	−3.30	0.07	0.15	0.00	0.00
Li I	1	<0.43	...	...	...	...	...
C (CH)	1	4.53	−0.60	0.15	0.25	0.19	0.19
N (NH)	1	5.48	1.29	0.30	0.36	0.32	0.32
O I	1	6.39	1.23	0.15	0.20	0.17	0.23
Na I	0	...	...	...	...	...	...
Mg I	8	4.67	0.60	0.06	0.16	0.09	0.17
Al I	1	2.33	−0.59	0.09	0.30	0.24	0.30
Si I	1	4.80	0.82	0.16	0.29	0.22	0.25
K I	0	...	...	...	...	...	...
Ca I	13	3.30	0.49	0.11	0.17	0.12	0.20
Sc II	6	−0.19	−0.05	0.06	0.15	0.17	0.09
Ti I	10	1.75	0.33	0.05	0.14	0.08	0.18
Ti II	24	1.89	0.23	0.05	0.14	0.16	0.09
V I	1	0.38	−0.02	0.13	0.18	0.14	0.21
V II	2	0.67	0.04	0.20	0.24	0.26	0.21
Cr I	5	1.87	−0.24	0.06	0.15	0.08	0.18
Cr II	1	2.41	0.07	0.09	0.17	0.19	0.12
Mn I	4	1.41	−0.50	0.08	0.17	0.11	0.20
Mn II	2	1.37	−0.76	0.16	0.21	0.23	0.17
Co I	3	1.45	−0.01	0.12	0.19	0.14	0.22
Ni I	3	2.69	−0.01	0.11	0.19	0.13	0.21
Cu I	0	...	...	...	...	...	...
Zn I	2	1.66	0.62	0.08	0.15	0.10	0.19
Ga I	0	...	...	...	...	...	...
Rb I	1	<1.51	<2.52	...	...	...	...
Sr II	2	−0.78	−0.35	0.04	0.25	0.24	0.26
Y II	4	−1.76	−0.67	0.11	0.18	0.20	0.13
Zr II	3	−0.79	−0.07	0.09	0.16	0.19	0.11
Nb II	1	<0.15	<1.99	...	...	...	...
Mo I	1	<−0.29	<1.36	...	...	...	...
Tc I	1	<−0.13	...	...	...	...	...
Ru I	0	...	...	...	...	...	...
Sn I	1	<0.81	<2.27	...	...	...	...
Ba II	3	−1.72	−0.60	0.07	0.15	0.17	0.10
La II	1	−2.47	−0.27	0.18	0.22	0.24	0.19
Ce II	5	<−1.76	<−0.04	...	...	...	...
Pr II	1	<−2.35	<0.23	...	...	...	...
Nd II	1	−2.26	−0.38	0.21	0.25	0.27	0.22
Sm II	2	<−1.78	<0.56	...	...	...	...
Eu II	4	<−3.05	<−0.27	...	...	...	...
Gd II	3	<−1.40	<0.83	...	...	...	...
Tb II	3	<−2.23	<0.77	...	...	...	...
Dy II	3	<−2.21	<−0.01	...	...	...	...
Ho II	1	<−2.22	<0.60	...	...	...	...
Er II	2	<−2.05	<0.33	...	...	...	...
Tm II	2	<−2.38	<0.82	...	...	...	...
Yb II	0	...	...	...	...	...	...
Hf II	2	<−1.26	<1.19	...	...	...	...
Ir I	1	<−0.64	<1.51	...	...	...	...
Pb I	1	<0.32	<1.81	...	...	...	...
Th II	2	<−2.26	<0.98	...	...	...	...

Note. [a] [Fe/H] is indicated for Fe I and Fe II.

CEMP-no and NEMP-no stars are low enough that relatively small numbers of supernovae can be expected to have pre-enriched the gas from which they formed. Yet the metallicities are high enough that elements heavier than the iron group can still be detected.

Our CEMP-no sample is shown by the shaded histogram in Figure 4. Our NEMP-no sample, comprised of the five stars with [N/Fe] > +1.0 and low [C/Fe] is shown by the hatched black histogram. A two-sided Kolmogorov–Smirnov (K-S) test rejects the null hypothesis that the metallicity distributions of the CEMP-no and NEMP-no samples are drawn from the same distribution at the 77% confidence level. Figure 5 shows similar histograms for the [Sr/Fe] and [Ba/Fe] ratios. For [Sr/Fe], [Ba/Fe], and [Sr/Ba] (not shown in Figure 5), the two-sided K-S test rejects the null hypothesis that the CEMP-no and NEMP-no samples are drawn from the same distribution at the 8%,

Table 8
Mean Abundances in CS 22891–200

Species	N_{lines}	$\log\epsilon$	[X/Fe][a]	$\sigma_{statistical}$	σ_{total}	$\sigma_{neutrals}$	σ_{ions}
Fe I	87	3.44	−4.06	0.06	0.15	0.00	0.00
Fe II	9	3.62	−3.88	0.08	0.16	0.00	0.00
Li I	1	<0.13	...	...	...	...	...
C (CH)	1	4.90	0.35	0.15	0.25	0.19	0.20
N (NH)	1	5.15	1.20	0.30	0.36	0.32	0.33
O I	4	<6.30	<1.67	...	...	...	...
Na I	0	...	...	...	...	...	...
Mg I	9	4.36	0.82	0.06	0.16	0.09	0.18
Al I	1	2.02	−0.37	0.09	0.28	0.23	0.30
Si I	1	4.50	1.05	0.16	0.20	0.17	0.24
K I	1	1.29	0.32	0.19	0.23	0.20	0.26
Ca I	12	3.05	0.77	0.11	0.17	0.13	0.21
Sc II	5	−1.18	−0.45	0.07	0.15	0.18	0.11
Ti I	9	1.14	0.25	0.07	0.15	0.09	0.19
Ti II	24	1.21	0.14	0.07	0.15	0.18	0.11
V I	0	...	...	...	...	...	...
V II	1	0.05	−0.00	0.23	0.27	0.29	0.24
Cr I	4	1.15	−0.43	0.04	0.15	0.08	0.19
Cr II	0	...	...	...	...	...	...
Mn I	3	0.35	−1.02	0.05	0.14	0.08	0.18
Mn II	1	0.50	−1.05	0.32	0.35	0.36	0.33
Co I	6	0.75	−0.18	0.13	0.19	0.15	0.22
Ni I	4	2.02	−0.14	0.12	0.20	0.14	0.23
Cu I	0	...	...	...	...	...	...
Zn I	2	<1.37	<0.87	...	...	...	...
Ga I	0	...	...	...	...	...	...
Rb I	0	...	...	...	...	...	...
Sr II	2	−2.37	−1.36	0.04	0.15	0.17	0.11
Y II	2	−2.85	−1.18	0.19	0.24	0.25	0.21
Zr II	0	...	...	...	...	...	...
Nb II	1	<−0.22	<2.20	...	...	...	...
Mo I	1	<−0.86	<1.32	...	...	...	...
Tc I	1	<−0.68	...	...	...	...	...
Ru I	0	...	...	...	...	...	...
Sn I	0	...	...	...	...	...	...
Ba II	2	−2.63	−0.93	0.06	0.15	0.18	0.10
La II	0	...	...	...	...	...	...
Ce II	5	<−2.07	<0.23	...	...	...	...
Pr II	4	<−2.64	<0.52	...	...	...	...
Nd II	5	<−2.30	<0.16	...	...	...	...
Sm II	2	<−1.97	<0.95	...	...	...	...
Eu II	2	−3.43	−0.07	0.17	0.22	0.24	0.19
Gd II	2	<−1.65	<1.16	...	...	...	...
Tb II	3	<−2.34	<1.24	...	...	...	...
Dy II	3	<−2.44	<0.34	...	...	...	...
Ho II	1	<−2.65	<0.75	...	...	...	...
Er II	2	<−2.30	<0.66	...	...	...	...
Tm II	2	<−2.61	<1.17	...	...	...	...
Yb II	1	<−3.18	<−0.22	...	...	...	...
Hf II	2	<−1.41	<1.62	...	...	...	...
Ir I	1	<−0.85	<1.83	...	...	...	...
Pb I	1	<0.15	<2.17	...	...	...	...
Th II	3	<−2.46	<1.36	...	...	...	...

Note. [a] [Fe/H] is indicated for Fe I and Fe II.

Table 9
Mean Abundances in CS 22893–010

Species	N_{lines}	$\log\epsilon$	[X/Fe][a]	$\sigma_{statistical}$	σ_{total}	$\sigma_{neutrals}$	σ_{ions}
Fe I	112	4.38	−3.12	0.06	0.15	0.00	0.00
Fe II	9	4.57	−2.93	0.07	0.16	0.00	0.00
Li I	1	2.57	...	0.05	0.23	0.17	0.25
C (CH)	1	5.62	0.13	0.15	0.25	0.19	0.19
N (NH)	1	6.44	1.55	0.30	0.36	0.32	0.32
O I	1	6.58	1.01	0.12	0.18	0.13	0.21
Na I	2	4.70	1.58	0.11	0.17	0.12	0.20
Mg I	7	5.04	0.56	0.05	0.15	0.08	0.18
Al I	1	2.94	−0.39	0.09	0.29	0.23	0.30
Si I	1	5.24	0.85	0.16	0.29	0.22	0.26
K I	2	2.34	0.43	0.13	0.19	0.15	0.22
Ca I	14	3.70	0.48	0.11	0.17	0.12	0.20
Sc II	3	0.27	0.05	0.05	0.14	0.17	0.09
Ti I	7	2.15	0.32	0.07	0.15	0.09	0.18
Ti II	21	2.23	0.21	0.06	0.15	0.17	0.10
V I	0	...	...	...	...	...	...
V II	2	1.05	0.05	0.23	0.27	0.28	0.24
Cr I	5	2.33	−0.19	0.06	0.14	0.08	0.18
Cr II	0	...	...	...	...	...	...
Mn I	4	1.92	−0.39	0.09	0.16	0.11	0.20
Mn II	0	...	...	...	...	...	...
Co I	5	2.03	0.16	0.13	0.19	0.14	0.22
Ni I	2	3.13	0.03	0.11	0.18	0.13	0.21
Cu I	0	...	...	...	...	...	...
Zn I	3	<2.03	<0.59	...	...	...	...
Ga I	0	...	...	...	...	...	...
Rb I	1	<2.15	<2.75	...	...	...	...
Sr II	2	−0.29	−0.23	0.04	0.22	0.22	0.21
Y II	2	−1.45	−0.73	0.15	0.20	0.22	0.16
Zr II	1	−0.68	−0.33	0.15	0.20	0.22	0.16
Nb II	1	<1.02	<2.49	...	...	...	...
Mo I	1	<0.43	<1.67	...	...	...	...
Tc I	1	<0.67	...	...	...	...	...
Ru I	0	...	...	...	...	...	...
Sn I	0	...	...	...	...	...	...
Ba II	1	−2.03	−1.28	0.05	0.15	0.18	0.09
La II	0	...	...	...	...	...	...
Ce II	5	<−0.77	<0.58	...	...	...	...
Pr II	2	<−1.20	<1.01	...	...	...	...
Nd II	5	<−1.00	<0.51	...	...	...	...
Sm II	2	<−0.96	<1.01	...	...	...	...
Eu II	4	<−2.02	<0.39	...	...	...	...
Gd II	3	<−0.51	<1.35	...	...	...	...
Tb II	2	<−0.92	<1.71	...	...	...	...
Dy II	1	<−1.04	<0.79	...	...	...	...
Ho II	1	<−1.09	<1.36	...	...	...	...
Er II	3	<−1.01	<1.00	...	...	...	...
Tm II	2	<−1.22	<1.61	...	...	...	...
Yb II	1	<−1.86	<0.15	...	...	...	...
Hf II	2	<−0.20	<1.88	...	...	...	...
Ir I	0	...	...	...	...	...	...
Pb I	0	...	...	...	...	...	...
Th II	0	...	...	...	...	...	...

Note. [a] [Fe/H] is indicated for Fe I and Fe II.

46%, and 14% confidence levels. These tests indicate that the CEMP-no and NEMP-no samples do not exhibit significantly different distributions of [Fe/H], [Sr/Fe], [Ba/Fe], and [Sr/Ba].

We also examine whether the [Sr/Fe], [Ba/Fe], or [Sr/Ba] distributions in the CEMP-no, NEMP-no, or combined sample are different than "normal" stars in the Roederer et al. (2014) comparison sample. We exclude from the Roederer et al. sample all stars that are carbon- or *s*-process rich, are included in the CEMP-no or NEMP-no samples, or lack detection of both Sr II and Ba II lines. This leaves 266 stars for comparison. When comparing [Sr/Fe] in the CEMP-no and normal samples, for example, we select 11 stars at random from the normal sample. We then perform a K-S test on the [Sr/Fe] distributions in the CEMP-no and this subset of 11 normal stars to calculate the probability of rejecting the null hypothesis that these samples are drawn from the same distribution.

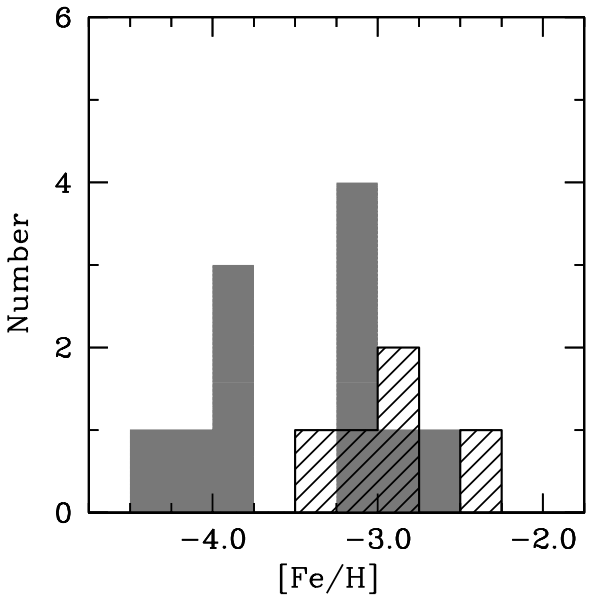

Figure 4. Metallicity distribution of our sample. The gray shaded histogram represents the 11 carbon-enhanced stars and the hatched histogram represents the 5 stars that are nitrogen-enhanced but not carbon-enhanced.

We conduct 1000 such trials, finding that the null hypothesis can be rejected only at the 76% confidence level on average. Similar tests conducted for [Sr/Fe] in the NEMP-no and combined samples can reject the null hypothesis at only the 41% and 80% confidence levels. For [Ba/Fe] in the CEMP-no, NEMP-no, and combined samples, this test can only reject the null hypothesis at the 88%, 42%, and 87% confidence levels. For [Sr/Ba] in the CEMP-no, NEMP-no, and combined samples, this test can only reject the null hypothesis at the 32%, 52%, and 43% confidence levels.

In summary, the CEMP-no, NEMP-no, and normal star samples are not distinct from one another from the perspective of the distributions of [Sr/Fe], [Ba/Fe], or [Sr/Ba] ratios. We will thus proceed to analyze both the CEMP-no and NEMP-no samples identically. Discussion of the heavy elements in the stars without carbon- and nitrogen enhancements is deferred for future work.

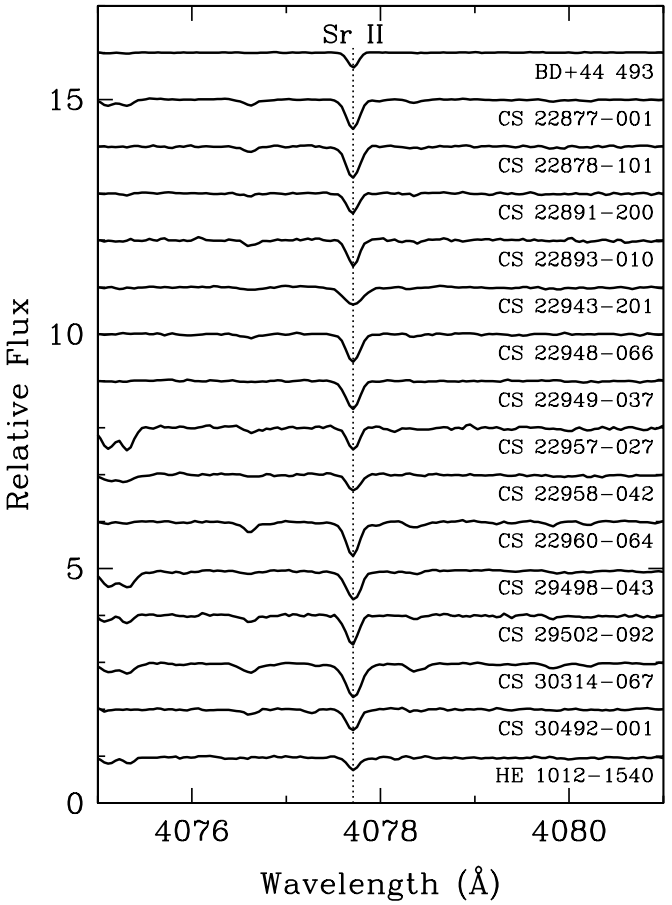

Figure 6. Spectra of the Sr II 4077 Å line for all 16 stars in our sample. The spectra have been offset vertically by intervals of 1.0.

4.2. Detection of Strontium and Barium

We detect strontium in all 16 stars. Figure 6 illustrates the spectral region around the Sr II 4077 Å line. We detect barium in 15 stars, as shown in Figure 7. At the scale shown in Figure 7, the Ba II 4554 Å line is difficult to see in BD+44 493, CS 22958–042, and HE 1012−1540, so Figure 8 illustrates these spectra

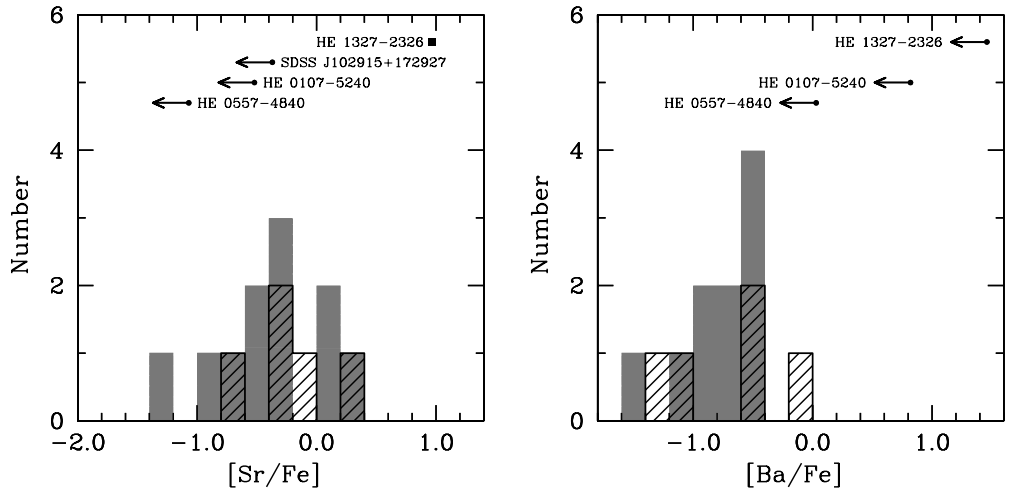

Figure 5. [Sr/Fe] and [Ba/Fe] distributions of our sample. The gray shaded histogram represents the 11 carbon-enhanced stars and the hatched histogram represents the 5 stars that are nitrogen-enhanced but not carbon-enhanced. Abundances or upper limits for stars with [Fe/H] < −4.5 are also shown: HE 0557−4840 (Norris et al. 2007), HE 0107−5240 (Christlieb et al. 2004), SDSS J102915+172927 (Caffau et al. 2012), and HE 1327−2326 (Frebel et al. 2005; Aoki et al. 2006). No barium abundance or upper limit has been reported for SDSS J102915+172927.

Table 10
Mean Abundances in CS 22943–201

Species	N_{lines}	$\log\epsilon$	[X/Fe][a]	$\sigma_{statistical}$	σ_{total}	$\sigma_{neutrals}$	σ_{ions}
Fe I	72	4.82	−2.68	0.06	0.17	0.00	0.00
Fe II	8	4.81	−2.69	0.06	0.15	0.00	0.00
Li I	1	<2.04	...	...	...	...	...
C (CH)	1	7.63	1.89	0.15	0.25	0.19	0.19
N (NH)	1	<6.70	<1.56	...	...	...	...
O I	3	6.25	0.24	0.08	0.18	0.10	0.20
Na I	0	...	...	...	...	...	...
Mg I	7	5.54	0.63	0.05	0.17	0.08	0.20
Al I	1	3.10	−0.67	0.09	0.18	0.11	0.21
Si I	0	...	...	...	...	...	...
K I	0	...	...	...	...	...	...
Ca I	11	4.19	0.53	0.11	0.19	0.12	0.21
Sc II	4	0.15	−0.31	0.10	0.17	0.21	0.12
Ti I	3	2.70	0.43	0.07	0.17	0.10	0.20
Ti II	12	2.38	0.11	0.05	0.15	0.19	0.08
V I	0	...	...	...	...	...	...
V II	2	<1.59	<0.35	...	...	...	...
Cr I	4	2.81	−0.15	0.08	0.18	0.10	0.20
Cr II	1	2.90	−0.05	0.11	0.18	0.22	0.13
Mn I	3	2.49	−0.25	0.06	0.17	0.08	0.19
Mn II	5	2.39	−0.35	0.16	0.21	0.25	0.17
Co I	3	2.38	0.07	0.13	0.20	0.14	0.22
Ni I	6	3.51	−0.03	0.14	0.21	0.15	0.23
Cu I	0	...	...	...	...	...	...
Zn I	2	<2.61	<0.73	...	...	...	...
Ga I	0	...	...	...	...	...	...
Rb I	1	<2.94	<3.10	...	...	...	...
Sr II	2	0.21	0.03	0.04	0.17	0.19	0.11
Y II	1	−0.75	−0.27	0.16	0.21	0.25	0.17
Zr II	1	0.29	0.40	0.07	0.16	0.20	0.10
Nb II	1	<1.24	<2.47	...	...	...	...
Mo I	1	<1.44	<2.24	...	...	...	...
Tc I	0	...	...	...	...	...	...
Ru I	0	...	...	...	...	...	...
Sn I	1	<2.82	<3.43	...	...	...	...
Ba II	1	−1.04	−0.53	0.05	0.15	0.19	0.08
La II	0	...	...	...	...	...	...
Ce II	5	<−0.04	<1.07	...	...	...	...
Pr II	2	<−0.65	<1.32	...	...	...	...
Nd II	5	<−0.38	<0.89	...	...	...	...
Sm II	2	<−0.37	<1.36	...	...	...	...
Eu II	3	<−1.43	<0.74	...	...	...	...
Gd II	2	<0.04	<1.66	...	...	...	...
Tb II	1	<0.20	<2.59	...	...	...	...
Dy II	2	<−0.48	<1.11	...	...	...	...
Ho II	1	<−0.72	<1.49	...	...	...	...
Er II	2	<−0.48	<1.29	...	...	...	...
Tm II	2	<−0.98	<1.61	...	...	...	...
Yb II	1	<−1.24	<0.53	...	...	...	...
Hf II	2	<0.33	<2.17	...	...	...	...
Ir I	0	...	...	...	...	...	...
Pb I	1	<1.86	<2.50	...	...	...	...
Th II	2	<−0.55	<2.08	...	...	...	...

Note. [a] [Fe/H] is indicated for Fe I and Fe II.

Table 11
Mean Abundances in CS 22948–066

Species	N_{lines}	$\log\epsilon$	[X/Fe][a]	$\sigma_{statistical}$	σ_{total}	$\sigma_{neutrals}$	σ_{ions}
Fe I	99	4.00	−3.50	0.06	0.15	0.00	0.00
Fe II	11	4.32	−3.18	0.07	0.16	0.00	0.00
Li I	1	<0.45	...	...	...	...	...
C (CH)	1	4.50	−0.74	0.15	0.25	0.19	0.19
N (NH)	1	5.69	1.05	0.30	0.36	0.32	0.32
O I	3	<6.57	<1.38	...	...	...	...
Na I	0	...	...	...	...	...	...
Mg I	9	4.56	0.46	0.06	0.15	0.08	0.18
Al I	2	2.28	−0.67	0.09	0.28	0.22	0.29
Si I	1	4.54	0.53	0.16	0.30	0.24	0.28
K I	0	...	...	...	...	...	...
Ca I	12	3.29	0.44	0.11	0.17	0.13	0.20
Sc II	9	0.05	0.08	0.06	0.15	0.17	0.10
Ti I	9	1.70	0.24	0.07	0.15	0.09	0.18
Ti II	27	1.85	0.08	0.06	0.15	0.17	0.10
V I	1	0.68	0.25	0.13	0.18	0.14	0.21
V II	2	1.01	0.26	0.20	0.24	0.26	0.21
Cr I	4	1.82	−0.32	0.04	0.15	0.08	0.19
Cr II	2	2.67	0.21	0.10	0.17	0.19	0.12
Mn I	5	1.85	−0.08	0.07	0.16	0.10	0.19
Mn II	1	2.06	−0.19	0.15	0.21	0.22	0.17
Co I	9	1.67	0.17	0.14	0.21	0.16	0.24
Ni I	9	2.86	0.14	0.12	0.23	0.17	0.24
Cu I	0	...	...	...	...	...	...
Zn I	2	1.58	0.51	0.11	0.17	0.13	0.20
Ga I	0	...	...	...	...	...	...
Rb I	1	<1.96	<2.94	...	...	...	...
Sr II	2	−0.98	−0.67	0.04	0.25	0.24	0.25
Y II	2	−1.84	−0.87	0.13	0.19	0.21	0.14
Zr II	2	−1.00	−0.40	0.14	0.20	0.22	0.16
Nb II	0	...	...	...	...	...	...
Mo I	1	<−0.36	<1.26	...	...	...	...
Tc I	1	<−0.08	...	...	...	...	...
Ru I	0	...	...	...	...	...	...
Sn I	1	<1.29	<2.72	...	...	...	...
Ba II	2	−2.15	−1.15	0.07	0.15	0.18	0.10
La II	0	...	...	...	...	...	...
Ce II	4	<−1.60	<0.00	...	...	...	...
Pr II	3	<−1.80	<0.66	...	...	...	...
Nd II	5	<−1.71	<0.05	...	...	...	...
Sm II	2	<−1.42	<0.80	...	...	...	...
Eu II	4	<−2.71	<−0.05	...	...	...	...
Gd II	3	<−1.13	<0.98	...	...	...	...
Tb II	3	<−1.78	<1.10	...	...	...	...
Dy II	3	<−1.77	<0.31	...	...	...	...
Ho II	0	...	...	...	...	...	...
Er II	3	<−1.68	<0.58	...	...	...	...
Tm II	2	<−2.10	<0.98	...	...	...	...
Yb II	0	...	...	...	...	...	...
Hf II	2	<−0.93	<1.40	...	...	...	...
Ir I	0	...	...	...	...	...	...
Pb I	1	<0.68	<2.14	...	...	...	...
Th II	3	<−1.94	<1.18	...	...	...	...

Note. [a] [Fe/H] is indicated for Fe I and Fe II.

on a magnified scale. The Ba II 4554 Å line is detected at the 7σ level in each of BD+44 493 and HE 1012−1540. Ito et al. (2013) and Cohen et al. (2008) also detected this line in their spectra of these stars. Meanwhile, the Ba II 4554 Å line is only detected at the 1.3σ level in CS 22958–042, which is not significant. CS 22958–042 is a warm subgiant ($T_{\rm eff}$ = 5760 K), and the 3σ upper limit derived from this line constrains [Ba/Fe] < −1.02. The [Ba/Fe] ratio is even lower in three stars in our sample, so it is possible that barium is present but not detected in CS 22958–042. The strontium and barium detections form our first main observational result: an element at or beyond the first neutron-capture peak (i.e., strontium) is detected in all stars, and an element at or beyond the second neutron-capture peak (i.e., barium) is detected in nearly all stars.

In contrast, other studies have shown that it is observationally challenging to detect strontium or barium in the four most

Table 12
Mean Abundances in CS 22949–037

Species	N_{lines}	$\log\epsilon$	[X/Fe][a]	$\sigma_{statistical}$	σ_{total}	$\sigma_{neutrals}$	σ_{ions}
Fe I	58	3.12	−4.38	0.07	0.15	0.00	0.00
Fe II	2	3.30	−4.20	0.07	0.16	0.00	0.00
Li I	1	<0.13	...	...	...	...	...
C (CH)	1	5.21	0.99	0.15	0.25	0.19	0.19
N (NH)	1	6.12	2.50	0.30	0.36	0.32	0.32
O I	2	<6.70	<2.39	...	...	...	...
Na I	0	...	...	...	...	...	...
Mg I	7	4.78	1.56	0.05	0.15	0.09	0.18
Al I	1	2.33	0.26	0.09	0.29	0.24	0.30
Si I	1	4.65	1.52	0.15	0.28	0.22	0.26
K I	0	...	...	...	...	...	...
Ca I	9	2.63	0.67	0.13	0.18	0.15	0.21
Sc II	5	−1.20	−0.14	0.08	0.16	0.19	0.12
Ti I	3	0.85	0.28	0.11	0.17	0.13	0.20
Ti II	14	0.94	0.19	0.06	0.15	0.18	0.10
V I	0	...	...	...	...	...	...
V II	2	<0.19	<0.46	...	...	...	...
Cr I	4	0.87	−0.39	0.06	0.15	0.10	0.18
Cr II	0	...	...	...	...	...	...
Mn I	3	0.41	−0.64	0.06	0.14	0.10	0.18
Mn II	0	...	...	...	...	...	...
Co I	3	0.81	0.19	0.12	0.18	0.14	0.21
Ni I	6	1.94	0.10	0.14	0.23	0.18	0.25
Cu I	0	...	...	...	...	...	...
Zn I	2	<1.40	<1.22	...	...	...	...
Ga I	0	...	...	...	...	...	...
Rb I	1	<1.65	<3.51	...	...	...	...
Sr II	2	−1.02	0.31	0.04	0.25	0.25	0.26
Y II	2	−2.25	−0.25	0.12	0.19	0.21	0.14
Zr II	2	−1.15	0.48	0.12	0.19	0.21	0.14
Nb II	1	<−0.10	<2.64	...	...	...	...
Mo I	1	<−0.52	<1.98	...	...	...	...
Tc I	0	...	...	...	...	...	...
Ru I	0	...	...	...	...	...	...
Sn I	1	<0.90	<3.21	...	...	...	...
Ba II	2	−2.80	−0.78	0.09	0.16	0.19	0.11
La II	0	...	...	...	...	...	...
Ce II	5	<−1.88	<0.74	...	...	...	...
Pr II	4	<−2.24	<1.24	...	...	...	...
Nd II	5	<−2.13	<0.65	...	...	...	...
Sm II	2	<−1.98	<1.26	...	...	...	...
Eu II	4	<−3.17	<0.51	...	...	...	...
Gd II	1	<−1.34	<1.79	...	...	...	...
Tb II	3	<−2.42	<1.48	...	...	...	...
Dy II	3	<−2.25	<0.85	...	...	...	...
Ho II	2	<−2.36	<1.36	...	...	...	...
Er II	3	<−2.09	<1.19	...	...	...	...
Tm II	2	<−2.62	<1.48	...	...	...	...
Yb II	0	...	...	...	...	...	...
Hf II	2	<−1.21	<2.14	...	...	...	...
Ir I	1	<−0.67	<2.33	...	...	...	...
Pb I	1	<0.32	<2.66	...	...	...	...
Th II	2	<−2.19	<1.95	...	...	...	...

Note. [a] [Fe/H] is indicated for Fe I and Fe II.

Table 13
Mean Abundances in CS 22957–027

Species	N_{lines}	$\log\epsilon$	[X/Fe][a]	$\sigma_{statistical}$	σ_{total}	$\sigma_{neutrals}$	σ_{ions}
Fe I	36	4.31	−3.19	0.06	0.14	0.00	0.00
Fe II	3	4.50	−3.00	0.07	0.16	0.00	0.00
Li I	1	<0.86	...	...	...	...	...
C (CH)	1	7.85	2.42	0.15	0.25	0.19	0.19
N (NH)	1	6.33	1.50	0.30	0.36	0.32	0.32
O I	3	<6.70	<1.20	...	...	...	...
Na I	3	4.03	0.98	0.12	0.20	0.15	0.22
Mg I	3	4.49	0.08	0.06	0.16	0.09	0.19
Al I	1	3.14	−0.12	0.09	0.30	0.24	0.30
Si I	0	...	...	...	...	...	...
K I	1	1.88	0.04	0.16	0.20	0.17	0.23
Ca I	3	3.46	0.32	0.11	0.17	0.12	0.20
Sc II	0	...	...	...	...	...	...
Ti I	2	2.08	0.32	0.07	0.15	0.09	0.18
Ti II	5	2.15	0.20	0.05	0.15	0.17	0.12
V I	0	...	...	...	...	...	...
V II	0	...	...	...	...	...	...
Cr I	1	2.32	−0.13	0.04	0.14	0.07	0.18
Cr II	0	...	...	...	...	...	...
Mn I	0	...	...	...	...	...	...
Mn II	2	2.12	−0.31	0.15	0.22	0.23	0.20
Co I	4	1.94	0.15	0.13	0.19	0.14	0.22
Ni I	4	3.00	−0.03	0.12	0.20	0.14	0.22
Cu I	0	...	...	...	...	...	...
Zn I	1	<2.02	<0.65	...	...	...	...
Ga I	0	...	...	...	...	...	...
Rb I	1	<2.20	<2.87	...	...	...	...
Sr II	1	−0.88	−0.75	0.05	0.18	0.19	0.16
Y II	0	...	...	...	...	...	...
Zr II	0	...	...	...	...	...	...
Nb II	0	...	...	...	...	...	...
Mo I	0	...	...	...	...	...	...
Tc I	0	...	...	...	...	...	...
Ru I	0	...	...	...	...	...	...
Sn I	0	...	...	...	...	...	...
Ba II	1	−1.82	−1.00	0.05	0.15	0.18	0.09
La II	0	...	...	...	...	...	...
Ce II	4	<−0.06	<1.36	...	...	...	...
Pr II	2	<−0.37	<1.91	...	...	...	...
Nd II	1	<−0.16	<1.42	...	...	...	...
Sm II	2	<−0.54	<1.50	...	...	...	...
Eu II	1	<−1.60	<0.88	...	...	...	...
Gd II	1	<−0.22	<1.71	...	...	...	...
Tb II	2	<−0.15	<2.55	...	...	...	...
Dy II	1	<0.11	<2.01	...	...	...	...
Ho II	0	...	...	...	...	...	...
Er II	1	<−0.11	<1.97	...	...	...	...
Tm II	1	<−0.04	<2.86	...	...	...	...
Yb II	1	<−1.69	<0.39	...	...	...	...
Hf II	1	<0.19	<2.34	...	...	...	...
Ir I	0	...	...	...	...	...	...
Pb I	1	<1.26	<2.41	...	...	...	...
Th II	0	...	...	...	...	...	...

Note. [a] [Fe/H] is indicated for Fe I and Fe II.

iron-poor stars known, those with [Fe/H] < −4.5. Three of these stars are carbon-enhanced, and two of these three are nitrogen-enhanced. The fourth star, SDSS J102915+172927, is not carbon- or nitrogen-enhanced, and no interesting upper limits have been placed on its oxygen abundance (Caffau et al. 2012). Barium has not been detected in any of these stars, and none of the upper limits constrains [Ba/Fe] to be sub-solar. By construction all stars in our sample show sub-solar [Ba/Fe]. Among these four stars, strontium has only been detected in HE 1327−2326, the most iron-poor star known, where [Sr/Fe] = +0.97 (Frebel et al. 2005; Aoki et al. 2006). [Sr/Fe] is constrained to be sub-solar in the other three stars, and the upper limits are within the range of [Sr/Fe] ratios found for our sample. These upper limits are marked in Figure 5. As noted previously by Aoki et al., the [Sr/Fe] ratios span a range greater than 2 dex in the four stars with [Fe/H] < −4.5. This is comparable to the range of [Sr/Fe] ratios found in our sample. This

Table 14
Mean Abundances in CS 22958–042

Species	N_{lines}	log ϵ	[X/Fe][a]	$\sigma_{statistical}$	σ_{total}	$\sigma_{neutrals}$	σ_{ions}
Fe I	19	4.10	−3.40	0.06	0.21	0.00	0.00
Fe II	1	4.51	−2.99	0.11	0.16	0.00	0.00
Li I	1	<1.33	...	...	...	...	...
C (CH)	1	7.59	2.15	0.15	0.25	0.19	0.21
N (CN)	1	7.09	2.25	0.20	0.28	0.23	0.25
O I	0	...	...	...	...	...	...
Na I	2	<4.73	<1.89	...	...	...	...
Mg I	3	4.95	0.74	0.05	0.23	0.08	0.23
Al I	1	2.80	−0.25	0.09	0.29	0.17	0.30
Si I	0	...	...	...	...	...	...
K I	0	...	...	...	...	...	...
Ca I	4	3.42	0.48	0.13	0.23	0.15	0.25
Sc II	0	...	...	...	...	...	...
Ti I	0	...	...	...	...	...	...
Ti II	5	1.92	−0.04	0.06	0.14	0.20	0.12
V I	0	...	...	...	...	...	...
V II	0	...	...	...	...	...	...
Cr I	1	2.25	0.01	0.06	0.20	0.09	0.22
Cr II	0	...	...	...	...	...	...
Mn I	1	1.76	−0.27	0.07	0.20	0.10	0.22
Mn II	0	...	...	...	...	...	...
Co I	1	1.74	0.15	0.17	0.25	0.18	0.27
Ni I	0	...	...	...	...	...	...
Cu I	1	<2.64	<1.85	...	...	...	...
Zn I	0	...	...	...	...	...	...
Ga I	0	...	...	...	...	...	...
Rb I	0	...	...	...	...	...	...
Sr II	2	−0.45	−0.33	0.04	0.14	0.20	0.13
Y II	0	...	...	...	...	...	...
Zr II	0	...	...	...	...	...	...
Nb II	1	<1.71	<3.24	...	...	...	...
Mo I	1	<1.27	<2.79	...	...	...	...
Tc I	1	<2.40	...	...	...	...	...
Ru I	0	...	...	...	...	...	...
Sn I	0	...	...	...	...	...	...
Ba II	2	<−1.83	<−1.02	...	...	...	...
La II	3	<−0.69	<1.20	...	...	...	...
Ce II	4	<0.10	<1.51	...	...	...	...
Pr II	0	...	...	...	...	...	...
Nd II	0	...	...	...	...	...	...
Sm II	0	...	...	...	...	...	...
Eu II	2	<−1.34	<1.13	...	...	...	...
Gd II	1	<0.21	<2.13	...	...	...	...
Tb II	0	...	...	...	...	...	...
Dy II	3	<−0.24	<1.65	...	...	...	...
Ho II	1	<−0.55	<1.96	...	...	...	...
Er II	1	<0.21	<2.28	...	...	...	...
Tm II	1	<0.44	<3.33	...	...	...	...
Yb II	1	<−0.37	<1.70	...	...	...	...
Hf II	2	<0.61	<2.75	...	...	...	...
Ir I	0	...	...	...	...	...	...
Pb I	1	<2.01	<3.37	...	...	...	...
Th II	0	...	...	...	...	...	...

Note. [a] [Fe/H] is indicated for Fe I and Fe II.

Table 15
Mean Abundances in CS 22960–064

Species	N_{lines}	log ϵ	[X/Fe][a]	$\sigma_{statistical}$	σ_{total}	$\sigma_{neutrals}$	σ_{ions}
Fe I	102	4.73	−2.77	0.05	0.14	0.00	0.00
Fe II	12	4.73	−2.77	0.07	0.15	0.00	0.00
Li I	1	<0.86	...	...	...	...	...
C (CH)	1	5.80	0.14	0.15	0.25	0.19	0.19
N (NH)	1	6.41	1.35	0.30	0.36	0.32	0.32
O I	3	<6.85	<0.93	...	...	...	...
Na I	2	3.80	0.33	0.10	0.30	0.24	0.29
Mg I	5	5.27	0.44	0.05	0.15	0.08	0.17
Al I	1	3.81	0.13	0.08	0.25	0.18	0.22
Si I	0	...	...	...	...	...	...
K I	1	2.62	0.36	0.12	0.18	0.14	0.21
Ca I	12	4.02	0.45	0.11	0.17	0.12	0.20
Sc II	6	0.37	−0.01	0.06	0.15	0.18	0.09
Ti I	18	2.41	0.23	0.06	0.14	0.08	0.18
Ti II	26	2.45	0.28	0.06	0.15	0.17	0.09
V I	1	1.01	−0.15	0.12	0.18	0.13	0.21
V II	2	1.21	0.05	0.20	0.25	0.26	0.21
Cr I	9	2.70	−0.17	0.05	0.14	0.08	0.18
Cr II	2	3.01	0.14	0.08	0.16	0.19	0.11
Mn I	4	2.28	−0.37	0.06	0.15	0.08	0.18
Mn II	5	2.24	−0.41	0.15	0.21	0.22	0.17
Co I	7	2.21	−0.01	0.14	0.22	0.16	0.24
Ni I	10	3.57	0.12	0.13	0.20	0.15	0.22
Cu I	1	<1.48	<0.06	...	...	...	...
Zn I	2	2.19	0.40	0.06	0.14	0.08	0.18
Ga I	0	...	...	...	...	...	...
Rb I	1	<2.29	<2.54	...	...	...	...
Sr II	2	0.34	0.25	0.04	0.24	0.23	0.25
Y II	4	−0.74	−0.18	0.10	0.17	0.19	0.12
Zr II	3	0.16	0.35	0.06	0.15	0.18	0.09
Nb II	1	<0.69	<2.00	...	...	...	...
Mo I	1	<0.10	<0.99	...	...	...	...
Tc I	1	<0.42	...	...	...	...	...
Ru I	0	...	...	...	...	...	...
Sn I	1	<1.34	<2.04	...	...	...	...
Ba II	4	−0.80	−0.20	0.06	0.15	0.17	0.09
La II	4	−1.52	0.15	0.15	0.20	0.22	0.16
Ce II	2	−1.17	0.02	0.25	0.29	0.30	0.26
Pr II	1	<−1.20	<0.85	...	...	...	...
Nd II	1	−1.25	0.10	0.10	0.17	0.20	0.12
Sm II	1	−1.50	0.31	0.17	0.22	0.24	0.18
Eu II	4	−1.91	0.35	0.08	0.16	0.19	0.11
Gd II	2	<−0.69	<1.01	...	...	...	...
Tb II	3	<−1.30	<1.17	...	...	...	...
Dy II	2	−1.07	0.60	0.10	0.17	0.20	0.12
Ho II	0	...	...	...	...	...	...
Er II	1	−1.46	0.39	0.18	0.23	0.25	0.20
Tm II	0	...	...	...	...	...	...
Yb II	1	−1.57	0.28	0.12	0.18	0.20	0.13
Hf II	1	<−0.60	<1.32	...	...	...	...
Ir I	0	...	...	...	...	...	...
Pb I	1	<0.78	<1.51	...	...	...	...
Th II	0	...	...	...	...	...	...

Note. [a] [Fe/H] is indicated for Fe I and Fe II.

forms our second main observational result: from the perspective of heavy elements ($Z \geqslant 38$), our sample could represent higher-metallicity analogs of the carbon- and nitrogen-enhanced stars with [Fe/H] < -4.5.

4.3. Light Elements

The abundance patterns of the light elements (lithium through the iron group) in our sample have been discussed in many of the studies referenced in Section 2. We build on those excellent studies by leveraging the large comparison sample of Roederer et al. (2014) to place the abundance patterns of the CEMP-no and NEMP-no stars in the context of other stars at similar metallicity and evolutionary state. This enables us to identify element ratios that are outliers relative to the majority of carbon-normal metal-poor stars. The advantage of this differential approach is that uncertainties related to the analysis techniques largely cancel out.

Table 16
Mean Abundances in CS 29498–043

Species	N_{lines}	$\log \epsilon$	[X/Fe][a]	$\sigma_{statistical}$	σ_{total}	$\sigma_{neutrals}$	σ_{ions}
Fe I	74	3.63	−3.87	0.06	0.15	0.00	0.00
Fe II	6	3.65	−3.85	0.08	0.16	0.00	0.00
Li I	1	<−0.05	...	...	...	...	...
C (CH)	1	7.31	2.72	0.15	0.25	0.19	0.20
N (NH)	1	5.70	1.71	0.30	0.36	0.32	0.33
O I	3	7.19	2.37	0.08	0.15	0.10	0.19
Na I	4	3.40	1.03	0.17	0.23	0.19	0.25
Mg I	5	5.51	1.78	0.05	0.18	0.11	0.18
Al I	1	3.33	0.75	0.08	0.25	0.19	0.23
Si I	1	4.72	1.08	0.25	0.28	0.26	0.31
K I	2	1.61	0.46	0.14	0.19	0.16	0.23
Ca I	9	3.00	0.54	0.11	0.17	0.13	0.21
Sc II	3	−0.77	−0.07	0.10	0.17	0.19	0.13
Ti I	9	1.18	0.10	0.07	0.15	0.09	0.19
Ti II	13	1.38	0.27	0.06	0.15	0.17	0.11
V I	0	...	...	...	...	...	...
V II	0	...	...	...	...	...	...
Cr I	4	1.48	−0.29	0.08	0.15	0.10	0.19
Cr II	0	...	...	...	...	...	...
Mn I	1	1.11	−0.45	0.11	0.17	0.13	0.21
Mn II	0	...	...	...	...	...	...
Co I	2	0.86	−0.26	0.11	0.18	0.13	0.21
Ni I	3	2.30	−0.04	0.13	0.19	0.15	0.22
Cu I	0	...	...	...	...	...	...
Zn I	2	1.24	0.56	0.11	0.17	0.13	0.21
Ga I	0	...	...	...	...	...	...
Rb I	1	<1.31	<2.66	...	...	...	...
Sr II	1	−0.90	0.08	0.04	0.24	0.24	0.26
Y II	2	−1.90	−0.26	0.13	0.19	0.21	0.15
Zr II	0	...	...	...	...	...	...
Nb II	0	...	...	...	...	...	...
Mo I	0	...	...	...	...	...	...
Tc I	0	...	...	...	...	...	...
Ru I	0	...	...	...	...	...	...
Sn I	0	...	...	...	...	...	...
Ba II	2	−2.18	−0.51	0.05	0.15	0.17	0.11
La II	1	<−3.02	<−0.27	...	...	...	...
Ce II	1	<−2.13	<0.14	...	...	...	...
Pr II	1	<−2.21	<0.92	...	...	...	...
Nd II	2	<−1.75	<0.68	...	...	...	...
Sm II	1	<−2.03	<0.86	...	...	...	...
Eu II	1	<−3.12	<0.21	...	...	...	...
Gd II	0	...	...	...	...	...	...
Tb II	2	<−2.07	<1.48	...	...	...	...
Dy II	1	<−1.75	<1.00	...	...	...	...
Ho II	0	...	...	...	...	...	...
Er II	1	<−1.88	<1.05	...	...	...	...
Tm II	1	<−1.75	<2.00	...	...	...	...
Yb II	1	<−3.40	<−0.47	...	...	...	...
Hf II	1	<−1.56	<1.44	...	...	...	...
Ir I	0	...	...	...	...	...	...
Pb I	1	<0.67	<2.50	...	...	...	...
Th II	0	...	...	...	...	...	...

Note. [a] [Fe/H] is indicated for Fe I and Fe II.

Table 17
Mean Abundances in CS 29502–092

Species	N_{lines}	$\log \epsilon$	[X/Fe][a]	$\sigma_{statistical}$	σ_{total}	$\sigma_{neutrals}$	σ_{ions}
Fe I	90	4.20	−3.30	0.06	0.15	0.00	0.00
Fe II	9	4.30	−3.20	0.07	0.15	0.00	0.00
Li I	1	<0.45	...	...	...	...	...
C (CH)	1	6.19	0.96	0.15	0.25	0.19	0.29
N (NH)	1	5.63	1.00	0.30	0.36	0.32	0.32
O I	3	6.52	1.13	0.16	0.20	0.17	0.23
Na I	1	2.92	−0.02	0.10	0.27	0.22	0.29
Mg I	8	4.80	0.51	0.05	0.16	0.09	0.18
Al I	1	2.55	−0.60	0.09	0.29	0.24	0.30
Si I	0	...	...	...	...	...	...
K I	1	1.99	0.26	0.15	0.20	0.16	0.22
Ca I	10	3.41	0.37	0.11	0.17	0.13	0.20
Sc II	3	−0.14	−0.10	0.06	0.15	0.17	0.09
Ti I	12	1.82	0.17	0.07	0.15	0.09	0.18
Ti II	20	1.87	0.12	0.06	0.15	0.17	0.10
V I	0	...	...	...	...	...	...
V II	2	0.72	−0.02	0.22	0.26	0.28	0.23
Cr I	8	2.19	−0.15	0.07	0.15	0.09	0.18
Cr II	2	2.65	0.21	0.10	0.17	0.19	0.12
Mn I	2	2.11	−0.02	0.06	0.14	0.08	0.18
Mn II	2	1.73	−0.50	0.15	0.21	0.23	0.17
Co I	5	1.73	0.04	0.15	0.21	0.17	0.24
Ni I	7	3.21	0.29	0.13	0.20	0.15	0.23
Cu I	0	...	...	...	...	...	...
Zn I	2	1.70	0.44	0.09	0.16	0.11	0.19
Ga I	0	...	...	...	...	...	...
Rb I	1	<1.70	<2.48	...	...	...	...
Sr II	2	−0.76	−0.44	0.04	0.24	0.24	0.24
Y II	2	−1.77	−0.79	0.12	0.19	0.21	0.14
Zr II	0	...	...	...	...	...	...
Nb II	1	<0.52	<2.26	...	...	...	...
Mo I	1	<0.07	<1.49	...	...	...	...
Tc I	1	<0.42	...	...	...	...	...
Ru I	0	...	...	...	...	...	...
Sn I	1	<1.26	<2.49	...	...	...	...
Ba II	2	−2.48	−1.46	0.09	0.17	0.19	0.12
La II	0	...	...	...	...	...	...
Ce II	5	<−1.44	<0.18	...	...	...	...
Pr II	1	<−1.75	<0.73	...	...	...	...
Nd II	5	<−1.61	<0.17	...	...	...	...
Sm II	2	<−1.53	<0.71	...	...	...	...
Eu II	1	<−2.67	<0.01	...	...	...	...
Gd II	2	<−1.04	<1.09	...	...	...	...
Tb II	3	<−1.60	<1.30	...	...	...	...
Dy II	2	<−1.60	<0.50	...	...	...	...
Ho II	1	<−1.83	<0.89	...	...	...	...
Er II	2	<−1.70	<0.58	...	...	...	...
Tm II	2	<−1.82	<1.28	...	...	...	...
Yb II	1	<−2.54	<−0.26	...	...	...	...
Hf II	2	<−0.78	<1.57	...	...	...	...
Ir I	1	<−0.14	<1.78	...	...	...	...
Pb I	1	<0.60	<1.86	...	...	...	...
Th II	0	...	...	...	...	...	...

Note. [a] [Fe/H] is indicated for Fe I and Fe II.

We identify all stars in the Roederer et al. (2014) sample that have similar T_{eff} and [Fe/H] to each CEMP-no or NEMP-no star in our sample. In most cases, we select comparison stars that have T_{eff} within ±200 K and [Fe/H] within ±0.3 dex. This typically yields 10–20 stars for comparison (minimum, 3 stars; maximum, 29 stars). In a few cases, we broaden the range of T_{eff} or [Fe/H] to include sufficient numbers of comparison stars. We exclude other CEMP-no or NEMP-no stars in our sample from the comparison samples, and we also exclude stars that exhibit high levels of *s*-process enrichment. This signature indicates pollution by a companion that passed through the TP-AGB phase of evolution, so the present-day abundances of these stars are not representative of the interstellar medium from which they formed.

The top panels of Figures 9 through 24 illustrate this comparison for all 16 stars in our sample. The number of comparison

Table 18
Mean Abundances in CS 30314–067

Species	N_{lines}	$\log\epsilon$	[X/Fe][a]	$\sigma_{statistical}$	σ_{total}	$\sigma_{neutrals}$	σ_{ions}
Fe I	91	4.19	−3.31	0.06	0.15	0.00	0.00
Fe II	8	4.49	−3.01	0.06	0.15	0.00	0.00
Li I	1	<−0.41	...	...	...	...	...
C (CH)	1	5.97	0.55	0.15	0.25	0.19	0.19
N (NH)	1	6.00	1.18	0.30	0.36	0.32	0.32
O I	3	6.49	1.11	0.21	0.25	0.22	0.27
Na I	0	...	...	...	...	...	...
Mg I	5	4.85	0.56	0.06	0.16	0.09	0.18
Al I	1	3.02	−0.12	0.08	0.24	0.16	0.19
Si I	1	5.25	1.05	0.16	0.30	0.24	0.30
K I	2	2.00	0.28	0.13	0.18	0.14	0.21
Ca I	10	3.48	0.45	0.11	0.17	0.12	0.20
Sc II	5	0.01	−0.13	0.05	0.14	0.17	0.08
Ti I	18	1.68	0.04	0.05	0.14	0.08	0.17
Ti II	21	2.21	0.27	0.04	0.14	0.17	0.08
V I	0	...	...	...	...	...	...
V II	2	0.83	−0.08	0.19	0.23	0.25	0.20
Cr I	9	2.06	−0.27	0.05	0.14	0.08	0.17
Cr II	3	2.80	0.17	0.08	0.16	0.19	0.10
Mn I	3	1.54	−0.58	0.06	0.14	0.08	0.18
Mn II	2	1.45	−0.97	0.14	0.26	0.25	0.24
Co I	5	1.13	−0.56	0.15	0.29	0.23	0.29
Ni I	7	2.97	0.05	0.13	0.18	0.14	0.21
Cu I	1	<0.27	<−0.61	...	...	...	...
Zn I	3	1.88	0.62	0.06	0.14	0.08	0.18
Ga I	0	...	...	...	...	...	...
Rb I	1	<1.22	<2.01	...	...	...	...
Sr II	1	−0.50	−0.36	0.03	0.18	0.17	0.19
Y II	4	−1.63	−0.83	0.09	0.17	0.19	0.11
Zr II	3	−0.52	−0.08	0.05	0.15	0.17	0.08
Nb II	0	...	...	...	...	...	...
Mo I	0	...	...	...	...	...	...
Tc I	0	...	...	...	...	...	...
Ru I	0	...	...	...	...	...	...
Sn I	0	...	...	...	...	...	...
Ba II	4	−1.38	−0.55	0.05	0.15	0.17	0.09
La II	4	−2.60	−0.69	0.13	0.19	0.21	0.14
Ce II	1	−2.06	−0.63	0.12	0.18	0.21	0.14
Pr II	1	<−2.25	<0.04	...	...	...	...
Nd II	4	−2.01	−0.42	0.11	0.18	0.20	0.13
Sm II	1	−2.55	−0.50	0.12	0.19	0.21	0.14
Eu II	1	−3.11	−0.62	0.09	0.17	0.19	0.11
Gd II	1	<−1.95	<−0.01	...	...	...	...
Tb II	2	<−2.42	<0.29	...	...	...	...
Dy II	1	<−2.73	<−0.82	...	...	...	...
Ho II	0	...	...	...	...	...	...
Er II	2	<−2.40	<−0.31	...	...	...	...
Tm II	1	<−2.06	<0.85	...	...	...	...
Yb II	1	−3.05	−0.96	0.16	0.21	0.23	0.17
Hf II	2	<−1.57	<0.59	...	...	...	...
Ir I	0	...	...	...	...	...	...
Pb I	1	<0.30	<1.57	...	...	...	...
Th II	0	...	...	...	...	...	...

Note. [a] [Fe/H] is indicated for Fe I and Fe II.

Table 19
Mean Abundances in CS 30492–001

Species	N_{lines}	$\log\epsilon$	[X/Fe][a]	$\sigma_{statistical}$	σ_{total}	$\sigma_{neutrals}$	σ_{ions}
Fe I	93	4.88	−2.62	0.06	0.21	0.00	0.00
Fe II	7	5.15	−2.35	0.07	0.14	0.00	0.00
Li I	1	2.02	...	0.06	0.20	0.09	0.20
C (CH)	1	6.03	−0.05	0.15	0.25	0.19	0.19
N (NH)	1	6.60	1.12	0.30	0.36	0.32	0.32
O I	3	6.72	0.64	0.10	0.21	0.12	0.22
Na I	1	3.47	−0.15	0.10	0.27	0.17	0.27
Mg I	6	5.45	0.47	0.05	0.22	0.08	0.21
Al I	2	2.96	−0.88	0.09	0.29	0.18	0.28
Si I	1	5.24	0.35	0.16	0.36	0.23	0.31
K I	0	...	...	...	...	...	...
Ca I	11	4.16	0.43	0.11	0.22	0.13	0.22
Sc II	3	0.92	0.12	0.05	0.13	0.20	0.09
Ti I	6	2.71	0.38	0.07	0.20	0.09	0.21
Ti II	21	2.89	0.30	0.07	0.14	0.20	0.10
V I	1	<1.65	<0.34	...	...	...	...
V II	1	1.86	0.28	0.20	0.24	0.28	0.22
Cr I	4	2.81	−0.22	0.05	0.22	0.09	0.22
Cr II	2	3.49	0.20	0.08	0.15	0.21	0.11
Mn I	4	2.52	−0.30	0.07	0.21	0.09	0.21
Mn II	2	2.61	−0.47	0.16	0.20	0.25	0.18
Co I	2	2.39	0.02	0.12	0.23	0.14	0.23
Ni I	5	3.67	0.06	0.13	0.26	0.16	0.25
Cu I	0	...	...	...	...	...	...
Zn I	2	2.16	0.22	0.14	0.23	0.15	0.24
Ga I	0	...	...	...	...	...	...
Rb I	1	<2.73	<2.83	...	...	...	...
Sr II	2	0.49	−0.03	0.04	0.24	0.25	0.24
Y II	2	−0.57	−0.43	0.13	0.18	0.24	0.15
Zr II	1	0.30	0.07	0.10	0.16	0.22	0.13
Nb II	1	<1.41	<2.30	...	...	...	...
Mo I	1	<1.09	<1.83	...	...	...	...
Tc I	1	<1.39	...	...	...	...	...
Ru I	0	...	...	...	...	...	...
Sn I	0	...	...	...	...	...	...
Ba II	2	−0.62	−0.45	0.07	0.14	0.20	0.10
La II	0	...	...	...	...	...	...
Ce II	5	<−0.02	<0.75	...	...	...	...
Pr II	1	<−0.25	<1.38	...	...	...	...
Nd II	5	<−0.06	<0.87	...	...	...	...
Sm II	2	<0.03	<1.42	...	...	...	...
Eu II	4	<−1.26	<0.57	...	...	...	...
Gd II	3	<0.25	<1.53	...	...	...	...
Tb II	0	...	...	...	...	...	...
Dy II	1	<−0.38	<0.87	...	...	...	...
Ho II	0	...	...	...	...	...	...
Er II	2	<−0.25	<1.18	...	...	...	...
Tm II	2	<−0.53	<1.72	...	...	...	...
Yb II	1	<−1.12	<0.31	...	...	...	...
Hf II	1	<0.73	<2.23	...	...	...	...
Ir I	0	...	...	...	...	...	...
Pb I	1	<1.71	<2.29	...	...	...	...
Th II	2	<−0.33	<1.96	...	...	...	...

Note. [a] [Fe/H] is indicated for Fe I and Fe II.

stars and the range in T_{eff} and [Fe/H] considered are given in each figure caption. For each light element X in each CEMP-no or NEMP-no star, the [X/Fe] ratio is compared to the mean and standard deviation of the [X/Fe] ratios for stars in the comparison sample. Multiple ionization states of the same element are indicated separately. Only detections are considered in the comparison sample, thus the means may be overestimated for a few elements (e.g., [N/Fe]).

These comparisons reveal that the [X/Fe] ratios for all elements from potassium through zinc ($19 \leqslant Z \leqslant 30$) in each CEMP-no or NEMP-no star do not differ by more than $\approx 2\sigma$ from the comparison samples. Most are alike at the 1σ level. The few $\approx 2\sigma$ differences do not show any consistent patterns from one star to another, and within each star they do not occur for elements adjacent in atomic number. Thus we conclude

Table 20
Mean Abundances in HE 1012−1540

Species	N_{lines}	$\log\epsilon$	[X/Fe][a]	$\sigma_{statistical}$	σ_{total}	$\sigma_{neutrals}$	σ_{ions}
Fe I	48	3.33	−4.17	0.07	0.16	0.00	0.00
Fe II	1	3.74	−3.76	0.14	0.20	0.00	0.00
Li I	1	<0.75	...	...	...	...	...
C (CH)	1	6.66	1.99	0.15	0.25	0.19	0.23
N (NH)	1	4.81	0.74	0.30	0.36	0.32	0.35
O I	2	<6.70	<2.18	...	...	...	...
Na I	2	3.72	1.65	0.10	0.29	0.23	0.32
Mg I	3	5.24	1.80	0.05	0.15	0.09	0.22
Al I	1	2.97	0.69	0.09	0.29	0.23	0.33
Si I	0	...	...	...	...	...	...
K I	1	<1.87	<1.01	...	...	...	...
Ca I	4	3.05	0.88	0.11	0.18	0.14	0.24
Sc II	1	<−0.68	<−0.07	...	...	...	...
Ti I	0	...	...	...	...	...	...
Ti II	5	0.58	−0.61	0.10	0.17	0.20	0.17
V I	0	...	...	...	...	...	...
V II	2	<1.30	<1.13	...	...	...	...
Cr I	1	1.12	−0.35	0.14	0.19	0.15	0.25
Cr II	0	...	...	...	...	...	...
Mn I	1	0.74	−0.52	0.08	0.15	0.11	0.22
Mn II	0	...	...	...	...	...	...
Co I	2	1.08	0.26	0.17	0.21	0.19	0.27
Ni I	5	2.00	−0.06	0.16	0.21	0.17	0.27
Cu I	0	...	...	...	...	...	...
Zn I	3	<1.90	<1.51	...	...	...	...
Ga I	1	<0.93	<2.06	...	...	...	...
Rb I	1	<2.06	<3.71	...	...	...	...
Sr II	2	−1.69	−0.80	0.05	0.15	0.18	0.15
Y II	6	<−1.63	<−0.08	...	...	...	...
Zr II	2	<−0.28	<0.90	...	...	...	...
Nb II	1	<0.94	<3.24	...	...	...	...
Mo I	1	<0.36	<2.65	...	...	...	...
Tc I	0	...	...	...	...	...	...
Ru I	0	...	...	...	...	...	...
Sn I	0	...	...	...	...	...	...
Ba II	1	−2.27	−0.69	0.07	0.16	0.19	0.16
La II	0	...	...	...	...	...	...
Ce II	5	<−0.71	<1.47	...	...	...	...
Pr II	3	<−1.32	<1.72	...	...	...	...
Nd II	4	<−0.92	<1.42	...	...	...	...
Sm II	2	<−0.79	<2.01	...	...	...	...
Eu II	4	<−2.05	<1.19	...	...	...	...
Gd II	2	<−0.29	<2.40	...	...	...	...
Tb II	2	<−1.05	<2.41	...	...	...	...
Dy II	3	<−1.32	<1.34	...	...	...	...
Ho II	1	<−1.22	<2.06	...	...	...	...
Er II	3	<−1.01	<1.83	...	...	...	...
Tm II	2	<−1.32	<2.34	...	...	...	...
Yb II	1	<−1.60	<1.24	...	...	...	...
Hf II	2	<−0.25	<2.66	...	...	...	...
Ir I	0	...	...	...	...	...	...
Pb I	1	<1.38	<3.51	...	...	...	...
Th II	0	...	...	...	...	...	...

Note. [a] [Fe/H] is indicated for Fe I and Fe II.

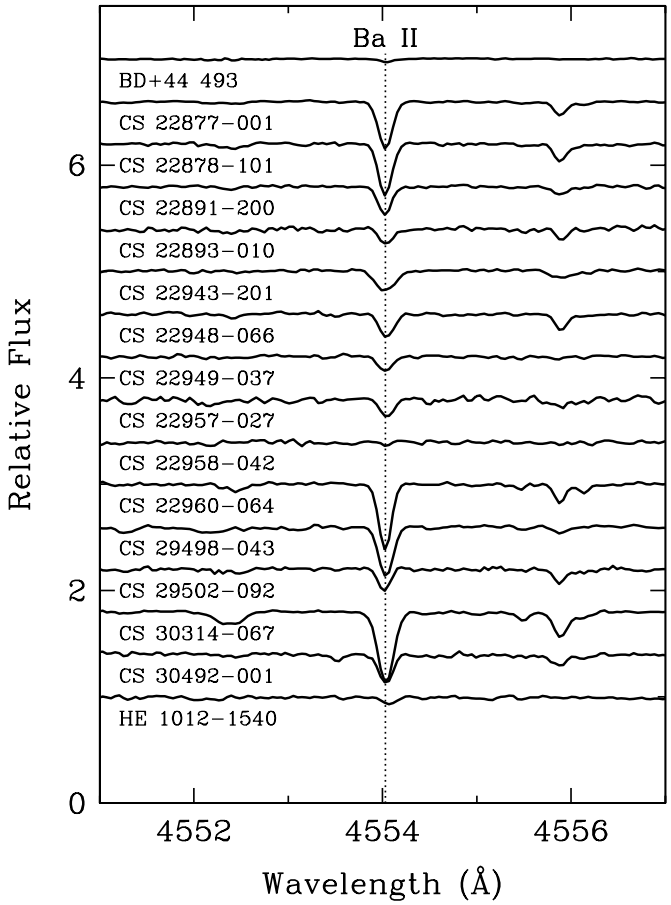

Figure 7. Spectra of the Ba II 4554 Å line for all 16 stars in our sample. The spectra have been offset vertically by intervals of 0.4.

Table 21
$^{12}C/^{13}C$ Ratios

Star	$^{12}C/^{13}C$
BD+44 493	>15
CS 22877–001	35 ± 15
CS 22878–101	...
CS 22891–200	>6
CS 22893–010	>5
CS 22943–201	>12
CS 22948–066	...
CS 22949–037	>4
CS 22957–027	6 ± 2
CS 22958–042	7 ± 2
CS 22960–064	15 ± 5
CS 29498–043	8 ± 3
CS 29502–092	12 ± 6
CS 30314–067	5 ± 1
CS 30492–001	...
HE 1012−1540	>30

that the elements from potassium to zinc are produced in similar proportions by the progenitors responsible for enriching the CEMP-no or NEMP-no stars and the comparison samples of halo stars. The [X/Fe] ratios for the iron-group elements in the CEMP-no and NEMP-no stars and comparison halo stars generally agree within factors of ≈2–3 with the iron group elements in HE 0107−5240, HE 1327−2326, and HE 0557−4840 (Christlieb et al. 2004; Aoki et al. 2006; Norris et al. 2007).

For the lighter elements oxygen, sodium, magnesium, aluminum, and silicon, at least one of these elements is >2σ higher in eight of the CEMP-no or NEMP-no stars than in the comparison samples. Three stars show more that one of these

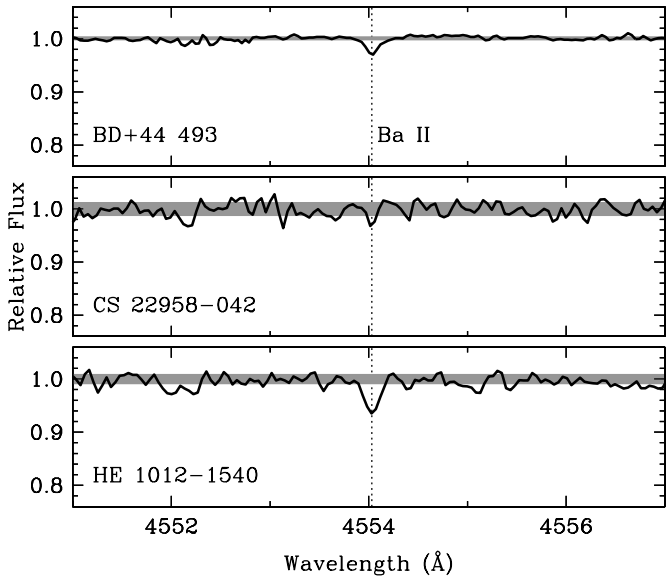

Figure 8. Spectra of the Ba II 4554 Å line for three stars with weak Ba II lines. The gray shaded bands illustrate the noise level in each spectrum. Although the Ba II line appears weak in BD+44 493, CS 22958–042, and HE 1012−1540, it is detected at the 7σ level in each of BD+44 493 and HE 1012−1540. This line is only detected at the 1.3σ level in CS 22958–042, which is not a significant detection.

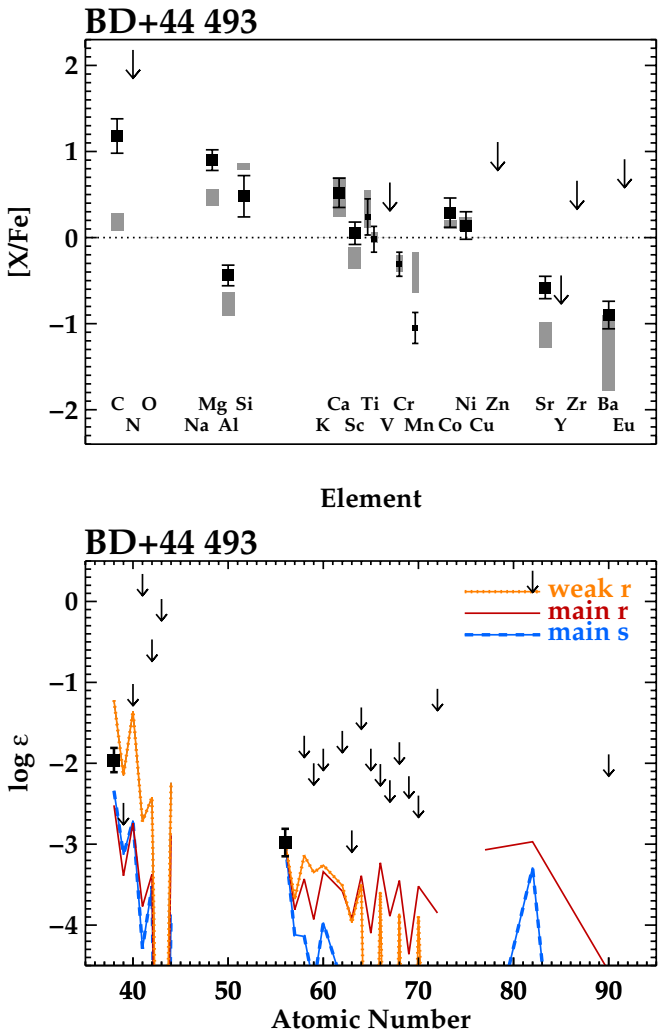

Figure 9. Top: comparison of abundances in BD+44 493 (filled black squares signifying detections or arrows signifying upper limits) with the average abundances of three other stars with $T_{\rm eff}$ within ±250 K and [Fe/H] within ±0.5 dex of BD+44 493. This comparison sample, shown by the shaded gray boxes, represents the mean $\pm1\sigma$ standard deviations. The comparison sample is only shown if it is derived from three or more stars. Smaller symbols are shown for titanium, vanadium, chromium, and manganese to accommodate ratios from both the neutral and ionized states, which may differ. The dotted line marks the solar ratios. Bottom: the heavy element distribution in BD+44 493. Filled squares mark detections, and arrows mark 3σ upper limits derived from non-detections. The studded orange line marks the scaled heavy element distribution found in the metal-poor giant HD 122563 (Honda et al. 2006; Roederer et al. 2012), frequently referred to as the distribution produced by the weak component of the *r*-process. The solid red line marks the scaled heavy element distribution found in the metal-poor giant CS 22892–052 (Sneden et al. 2003, 2009; Roederer et al. 2009), frequently associated with the distribution produced by the main component of the *r*-process. The long-dashed blue line marks the scaled heavy element distribution predicted by the main and strong components of the *s*-process (Sneden et al. 2008; Bisterzo et al. 2011). Each of the three curves has been renormalized to the barium abundance in BD+44 493.

(A color version of this figure is available in the online journal.)

elements high by $>2\sigma$, and three of these elements are high by $>2\sigma$ in two of these three stars. Enhanced levels of oxygen through silicon sometimes accompany the carbon and nitrogen enhancement. Previous studies have identified the similarity of potassium through zinc and the enhancement of oxygen through silicon in the CEMP-no and NEMP-no stars relative to carbon-normal stars. It is reassuring that these effects are confirmed by our analysis.

Figure 25 illustrates the lithium abundances of the CEMP-no and NEMP-no stars as a function of $T_{\rm eff}$. Lithium abundances for the full sample of halo stars analyzed by Roederer et al. (2014) are shown for comparison. Lithium is detected in 4 of the 16 stars. In 15 of the 16 stars, these abundances or upper limits fall within the range of lithium abundances or upper limits of the halo star sample. In one star, CS 22893–010 ($T_{\rm eff}$ = 5150 K), lithium is significantly enhanced, $\log\epsilon({\rm Li}) = +2.57 \pm 0.23$. For stars in a similar state of evolution on the red giant branch, the comparison sample shows $\log\epsilon({\rm Li}) \approx +1.0$. Nitrogen and sodium are significantly enhanced in CS 22893–010, [N/Fe] = +1.55 ± 0.36 and [Na/Fe] = +1.58 ± 0.17. No other element ratios in CS 22893–010 are different from the comparison star sample, as shown in Figure 13. Such enhanced [N/Fe] or [Na/Fe] ratios are not a universal feature of lithium-enhanced field giants (e.g., Lambert & Sawyer 1984; Ruchti et al. 2011b). A few such stars are found among the metal-poor red giants, but the [N/Fe] or [Na/Fe] enhancements are probably attributable to enrichment from an evolved companion (e.g., Roederer et al. 2008; Ruchti et al.). This does not appear to be the case with CS 22893–010.

Previous studies of lithium in (first ascent) red giant stars have typically shown that no more than ≈1% of these stars presently exhibit lithium enhancement relative to their peers (Brown et al. 1989; Pilachowski et al. 2000; Ruchti et al. 2011b; Kirby et al. 2012; Lebzelter et al. 2012; Martell & Shetrone 2013), although the mechanism that produces the lithium enhancement is not known with certainty. There are 98 red giant stars in the Roederer et al. sample, and our identification of one lithium-enhanced red giant is consistent with this frequency. If the lithium enhancement is not related to the nitrogen and sodium enhancement in CS 22893–010, we may conclude that nitrogen-(and carbon-)enhanced stars are also capable of going through a lithium-enhanced phase.

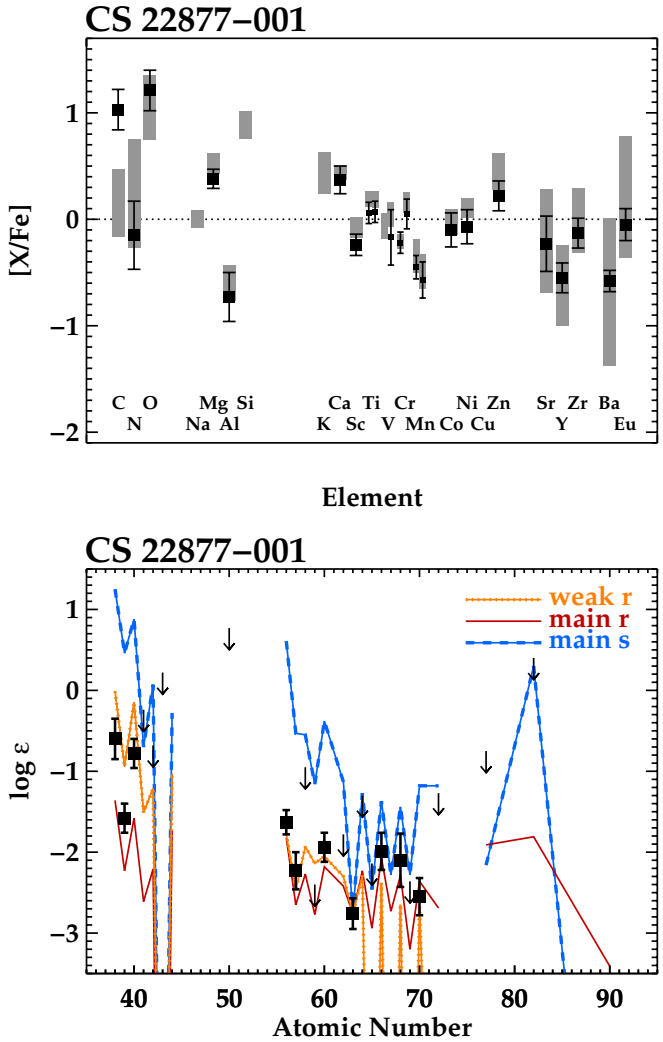

Figure 10. Top: comparison of abundances in CS 22877–001 with the average abundances of 24 other stars with $T_{\rm eff}$ within ±200 K and [Fe/H] within ±0.3 dex of CS 22877–001. Bottom: the heavy element distribution in CS 22877–001. Each of the three curves has been renormalized to the europium abundance in CS 22877–001. Symbols in both panels are the same as in Figure 9.
(A color version of this figure is available in the online journal.)

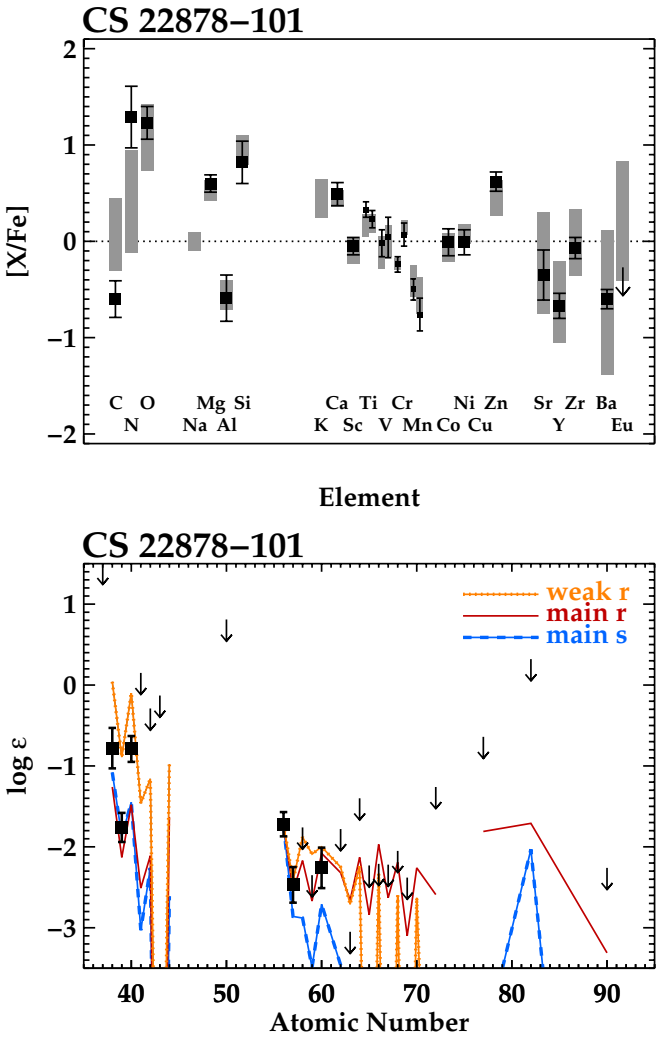

Figure 11. Top: comparison of abundances in CS 22878–101 with the average abundances of 18 other stars with $T_{\rm eff}$ within ±200 K and [Fe/H] within ±0.3 dex of CS 22878–101. Bottom: the heavy element distribution in CS 22878–101. Each of the three curves has been renormalized to the barium abundance in CS 22878–101. Symbols in both panels are the same as in Figure 9.
(A color version of this figure is available in the online journal.)

4.4. Elements Beyond the Iron Group

The top panels of Figures 9 through 24 illustrate the [Sr/Fe], [Y/Fe], [Zr/Fe], [Ba/Fe], and [Eu/Fe] ratios for all 16 stars in our sample with the comparison stars from the large sample of Roederer et al. (2014). The CEMP-no and NEMP-no stars do not appear unusual with respect to the carbon- and nitrogen-normal stars in this regard.

The bottom panels of Figures 9 through 24 illustrate the heavy element abundance patterns in these 16 stars. Three standard abundance patterns are shown for comparison. One pattern traces the heavy element abundances in the metal-poor halo star HD 122563, which has normal abundances of the lighter neutron-capture elements and a deficiency of the heaviest neutron-capture elements. The pattern found in this star may be considered representative of the weak component of the rapid neutron-capture process (the *r*-process). Another pattern traces the heavy element abundances in the *r*-process rich metal-poor halo star CS 22892–052, which is a well-known representative of a group of stars enriched by the main component of the *r*-process. The third pattern traces one outcome of *s*-process nucleosynthesis. This is derived from models of *s*-process nucleosynthesis in TP-AGB stars that are fit to the isotopic solar system *s*-process abundance pattern. In each figure, these patterns are rescaled to europium (if detected), or barium (if detected), or strontium.

We emphasize that these three curves are not intended to be rigid representations of distinct nucleosynthetic processes. Stars passing through the TP-AGB phase of evolution will produce different *s*-process abundance patterns that depend on the stellar mass, metallicity, mass loss rate, availability of neutrons from the $^{13}C(\alpha, n)^{16}O$ reaction, and so on. The abundance patterns produced by the weak and main components of the *r*-process may represent two extreme outcomes that result from variations in the physical conditions at the time of nucleosynthesis. While the general trends of these curves may help identify the nucleosynthetic processes responsible for creating the heavy elements in the CEMP-no and NEMP-no stars, we refrain from drawing conclusions from more detailed comparisons.

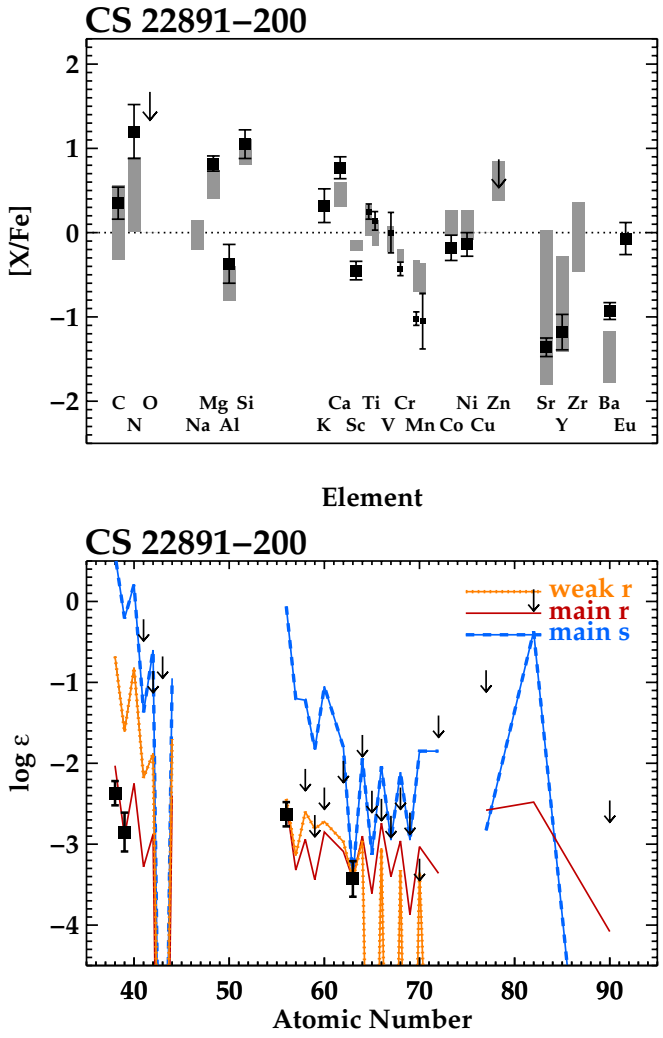

Figure 12. Top: comparison of abundances in CS 22891–200 with the average abundances of eight other stars with $T_{\rm eff}$ within ±200 K and [Fe/H] within ±0.3 dex of CS 22891–200. Bottom: the heavy element distribution in CS 22891–200. Each of the three curves has been renormalized to the europium abundance in CS 22891–200. Symbols in both panels are the same as in Figure 9.
(A color version of this figure is available in the online journal.)

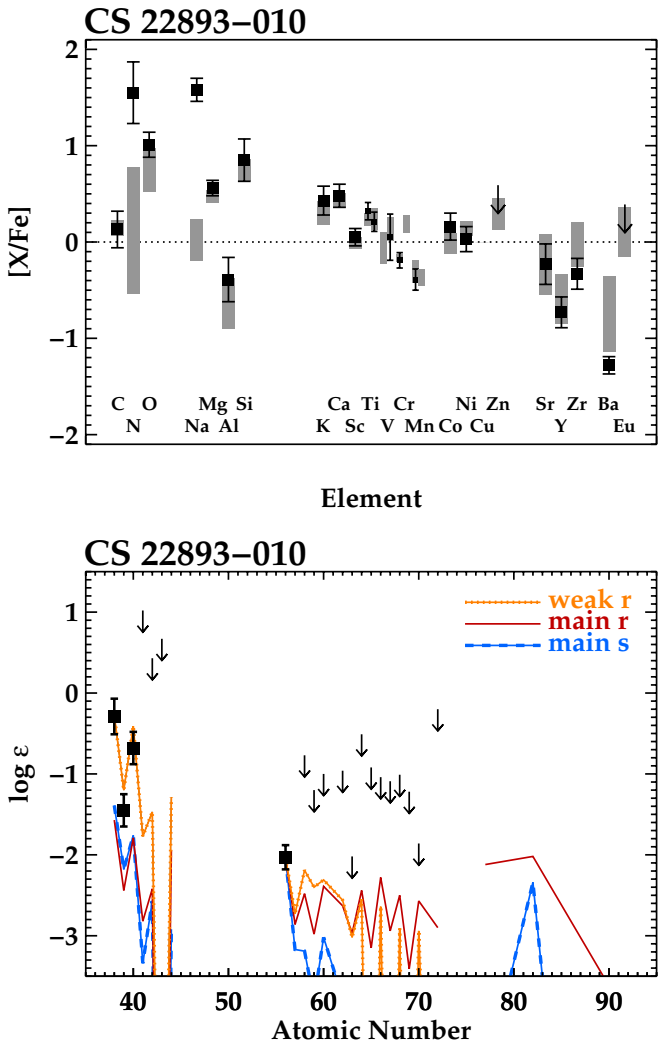

Figure 13. Top: comparison of abundances in CS 22893–010 with the average abundances of 12 other stars with $T_{\rm eff}$ within ±200 K and [Fe/H] within ±0.3 dex of CS 22893–010. Bottom: the heavy element distribution in CS 22893–010. Each of the three curves has been renormalized to the barium abundance in CS 22893–010. Symbols in both panels are the same as in Figure 9.
(A color version of this figure is available in the online journal.)

In five stars, sufficient numbers of key elements in the rare earth element domain[4] are detected, enabling us to assign a probable nucleosynthetic origin to their heavy elements. The pattern in CS 22891–200 (Figure 12) resembles the main component of the *r*-process as exemplified by CS 22892–052. CS 22877–001, CS 22960–064, and CS 30314–067 (Figures 10, 19, and 22) show patterns that resemble the weak component of the *r*-process as exemplified by HD 122563. The heavy element abundance pattern in CS 22878–101 shows evidence for at least a partial *s*-process origin. As shown in Figure 11, the upper limit on europium in CS 22878–101 is strong enough to rule out an exclusive *r*-process origin for the heavy elements, though a mix of *r*- and *s*-process material is possible. This star also exhibits a low level of radial velocity variations, suggesting that it may be in a binary system, and the unobserved companion could have passed through the TP-AGB phase of evolution and transferred a small, yet detectable, amount of *s*-process material to CS 22878–101.

Figure 26 illustrates the [Ba/Sr] ratio as a function of [Ba/Fe] for all 16 stars in our sample. The 5 stars whose neutron-capture patterns we can reliably assess are highlighted. The abscissa in Figure 26, [Ba/Fe], may be thought of as a dilution axis, reflecting the dilution of material produced by neutron-capture nucleosynthesis into differing amounts of iron. The ordinate in Figure 26, [Ba/Sr], may be thought of as reflecting properties intrinsic to the neutron-capture process itself.

CS 22891–200 is one of two stars in our sample with [Ba/Sr] > 0, and the pattern revealed by its strontium, yttrium, barium, and europium abundances is similar to that observed in the *r*-process rich standard star CS 22892–052 (Figure 12). [Ba/Sr] is also super-solar in HE 1012−1540. The [Ba/Sr] ratios in these 2 stars are similar to that found by Sneden et al. (2008) for 16 metal-poor stars with high levels of *r*-process enrichment, [Ba/Sr] = +0.3 ± 0.2 (see Figure 7 there). While carbon-enhanced stars with high levels of *r*-process enrichment

[4] The rare earth domain formally spans lanthanum through lutetium ($57 \leqslant Z \leqslant 71$) and includes scandium ($Z = 21$) and yttrium ($Z = 39$). For our purposes scandium and yttrium are irrelevant, but we extend the lanthanide range to include barium ($Z = 56$) and hafnium ($Z = 72$). Our working definition thus encompasses $56 \leqslant Z \leqslant 72$.

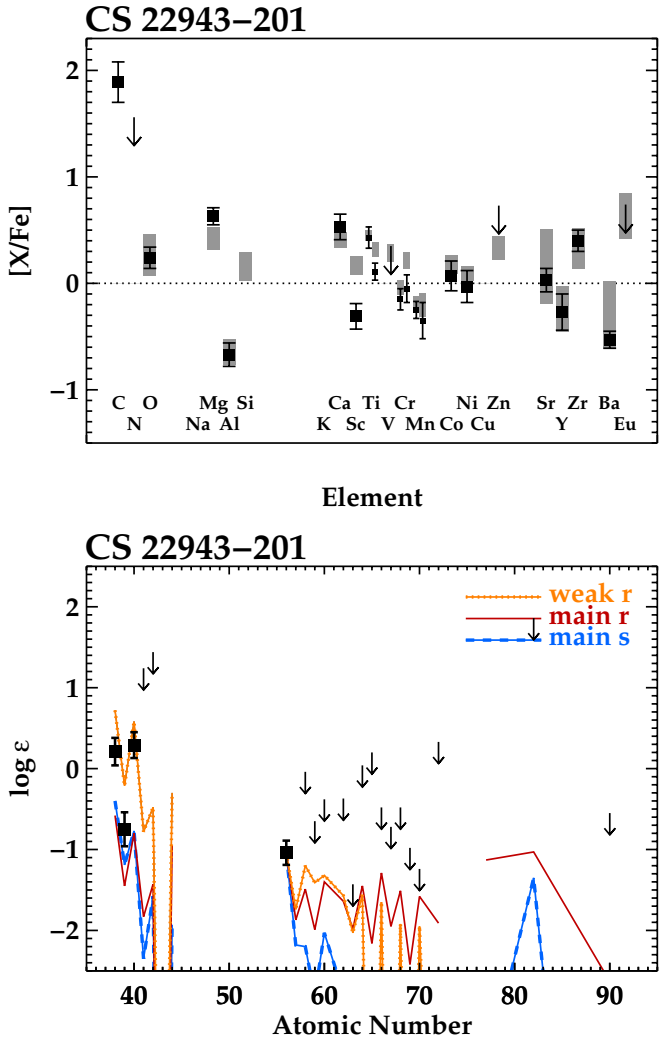

Figure 14. Top: comparison of abundances in CS 22943–201 with the average abundances of 11 other stars with $T_{\rm eff}$ within ±200 K and [Fe/H] within ±0.3 dex of CS 22943–201. Bottom: the heavy element distribution in CS 22943–201. Each of the three curves has been renormalized to the barium abundance in CS 22943–201. Symbols in both panels are the same as in Figure 9.
(A color version of this figure is available in the online journal.)

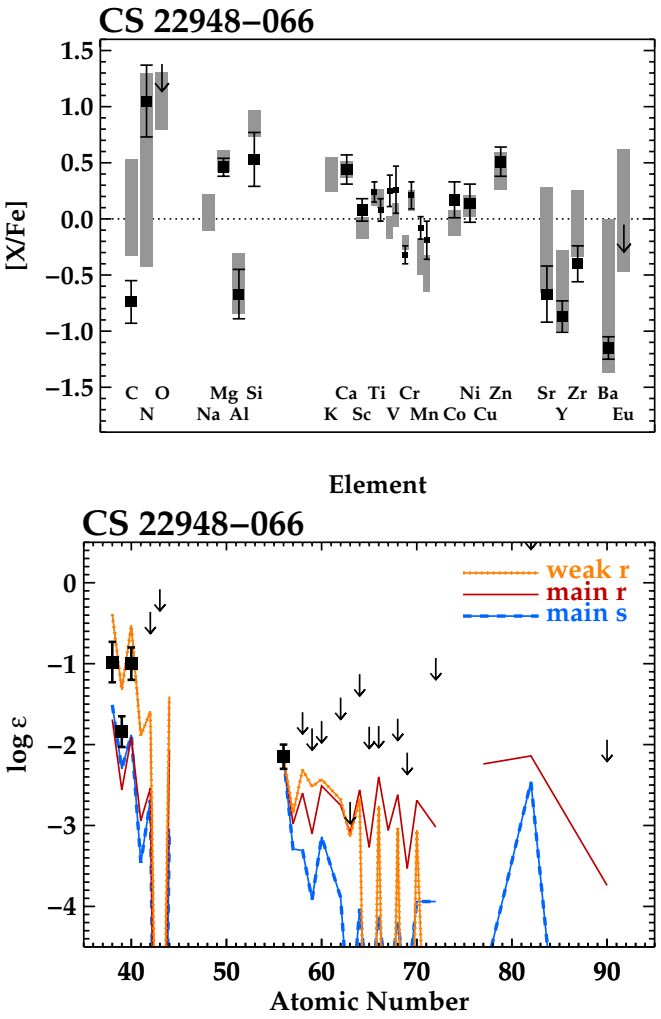

Figure 15. Top: comparison of abundances in CS 22948–066 with the average abundances of 29 other stars with $T_{\rm eff}$ within ±200 K and [Fe/H] within ±0.3 dex of CS 22948–066. Bottom: the heavy element distribution in CS 22948–066. Each of the three curves has been renormalized to the barium abundance in CS 22948–066. Symbols in both panels are the same as in Figure 9.
(A color version of this figure is available in the online journal.)

like CS 22892–052 would be excluded from our sample by the requirement that [Ba/Fe] < 0, we may consider CS 22891–200 and HE 1012−1540 to be related but enriched at a much lower level. Per hydrogen atom, europium atoms are approximately 100 times less common in CS 22891–200 than CS 22892–052, yet the ratios among the detected neutron-capture elements in these two stars are nearly identical. Finally, we point out that CS 22892–052 is also carbon- and nitrogen-enhanced, [C/Fe] = +0.88 and [N/Fe] = +1.01 (Sneden et al. 2003), though there is no consensus in the literature regarding the origin of its carbon, nitrogen, and *r*-process enhancement.

The three stars with patterns reminiscent of the weak component of the *r*-process show [Ba/Sr] ≈ −0.4 ± 0.2. Six of the stars whose neutron-capture patterns are yet unclassified also fall within this range (BD+44 493, CS 22943–201, CS 22948–066, CS 22957–027, CS 29498–043, CS 30492–001). The three stars we have classified are found on the right side of the diagram, where the overall neutron-capture element abundances are highest, thus affording us the best opportunity to detect other elements in the rare earth domain. It is therefore not surprising that the six unclassified stars with [Ba/Sr] ≈ −0.4 ± 0.2 have relatively low [Ba/Fe] ratios. The remaining four stars in Figure 26 show the lowest levels of [Ba/Sr] in our sample, [Ba/Sr] ≈ −1.0 (CS 22893–010, CS 22949–037, CS 22958–042, and CS 29502–092; note that CS 22958–042 shows an upper limit on barium that suggests membership in this group). It is possible that the 13 stars with [Ba/Sr] < 0 (except CS 22878–101) exhibit the results of a range of *r*-process nucleosynthetic conditions. We now consider alternative explanations.

In low-metallicity stars passing through the TP-AGB phase of evolution, *s*-process nucleosynthesis tends to produce [Ba/Fe] > 0 and [Ba/Sr] > 0. By construction, none of the stars in our sample fall into this regime. Some $^{12}C/^{13}C$ ratios of stars in our sample are low, but they are not uniformly as low as predicted by CN cycle equilibrium, $^{12}C/^{13}C \approx 3$–4. With the exception of CS 22878–101, this indicates that pollution by material produced in *s*-process nucleosynthesis and accompanied by CN-cycled material from an AGB star is not a likely origin of the strontium and barium in our sample.

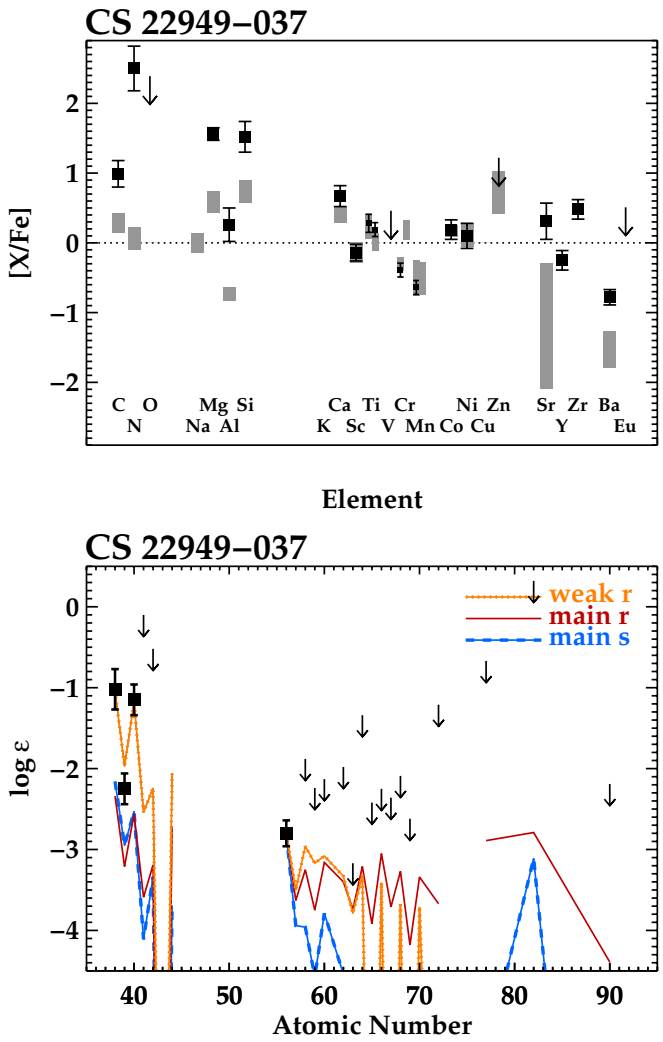

Figure 16. Top: comparison of abundances in CS 22949–037 with the average abundances of eight other stars with $T_{\rm eff}$ within ±200 K and [Fe/H] within ±0.5 dex of CS 22949–037. Bottom: the heavy element distribution in CS 22949–037. Each of the three curves has been renormalized to the barium abundance in CS 22949–037. Symbols in both panels are the same as in Figure 9.

(A color version of this figure is available in the online journal.)

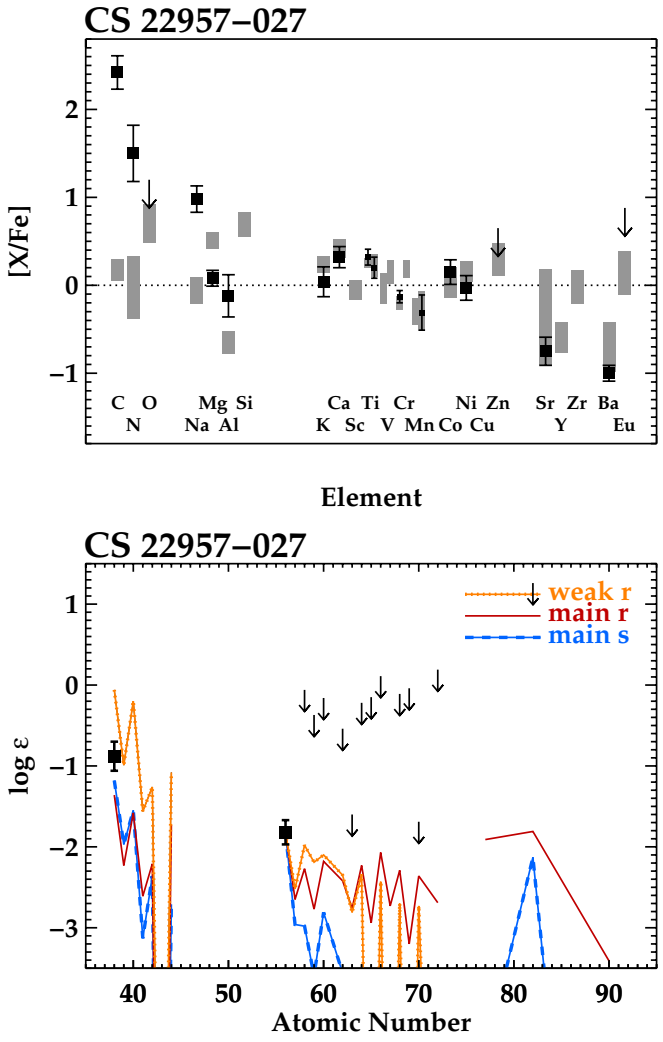

Figure 17. Top: comparison of abundances in CS 22957–027 with the average abundances of 11 other stars with $T_{\rm eff}$ within ±200 K and [Fe/H] within ±0.4 dex of CS 22957–027. Bottom: the heavy element distribution in CS 22957–027. Each of the three curves has been renormalized to the barium abundance in CS 22957–027. Symbols in both panels are the same as in Figure 9.

(A color version of this figure is available in the online journal.)

Lead (Pb, $Z = 82$) enjoys special status as the only readily observable element at the terminus of the *s*-process nucleosynthesis path. Enhanced lead is a clear signature of *s*-process nucleosynthesis in low-metallicity environments, where the high neutron-to-seed ratio drives the *s*-process flow to lead (e.g., Gallino et al. 1998). We do not detect lead in any star in our sample, and most of the upper limits are uninteresting, even in CS 22878–101. No upper limit approaches within an order of magnitude of the estimated minimum [Pb/Eu] ratio encountered in the case of *s*-process contributions ([Pb/Eu] ≈ +0.3; see Figure 2 of Roederer et al. 2010). Ito et al. (2013) report a stronger upper limit on lead in BD+44 493, but even this does not thoroughly exclude all traces of *s*-process material produced in a low-metallicity environment. Unfortunately, the observational limits on lead in these stars allow us only to say that prodigious lead production did not occur in the progenitors.

These considerations form our third main observational result: some form of *r*-process nucleosynthesis is responsible for the abundance patterns in four of the stars in our sample. The limited neutron-capture element abundance patterns in all but one of the remaining stars are consistent with an *r*-process origin, but the observations cannot offer compelling evidence against an *s*-process origin, either. The heavy elements in one star, CS 22878–101, suggest that material produced by *s*-process nucleosynthesis may be present. This result is not surprising, and it has long been suspected (e.g., Truran 1981) that *r*-process nucleosynthesis dominated the production of elements heavier than iron in the early Galaxy. Tumlinson's (2006) chemical evolution model predicts that the average field star with [Fe/H] = −3 and normal abundance ratios has ∼10 (zero-metallicity) progenitors, ranging anywhere from 1 to ≈20. While this prediction is difficult to test observationally, the unusual ratios of oxygen through silicon in the CEMP-no and NEMP-no stars hint that the number of progenitors should be on the low end of this range. Yet even in these stars, elements heavier than the iron group are found, and in some cases they appear to have been produced by *r*-process nucleosynthesis.

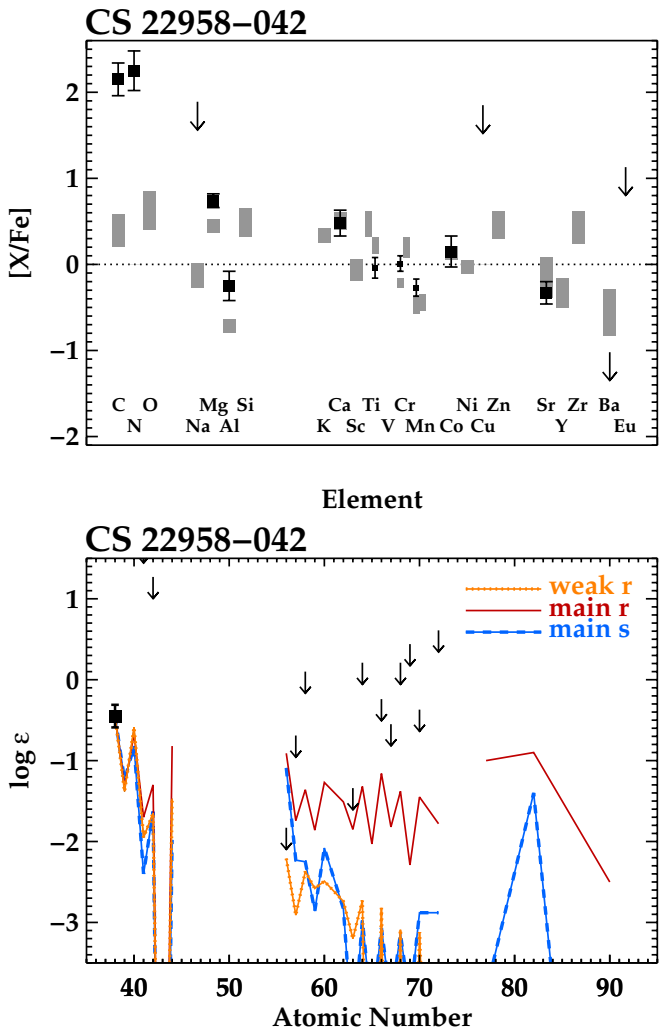

Figure 18. Top: comparison of abundances in CS 22958–042 with the average abundances of 28 other stars with $T_{\rm eff}$ within ±200 K and [Fe/H] within ±0.3 dex of CS 22958–042. Bottom: the heavy element distribution in CS 22958–042. Each of the three curves has been renormalized to the strontium abundance in CS 22958–042. Symbols in both panels are the same as in Figure 9.

(A color version of this figure is available in the online journal.)

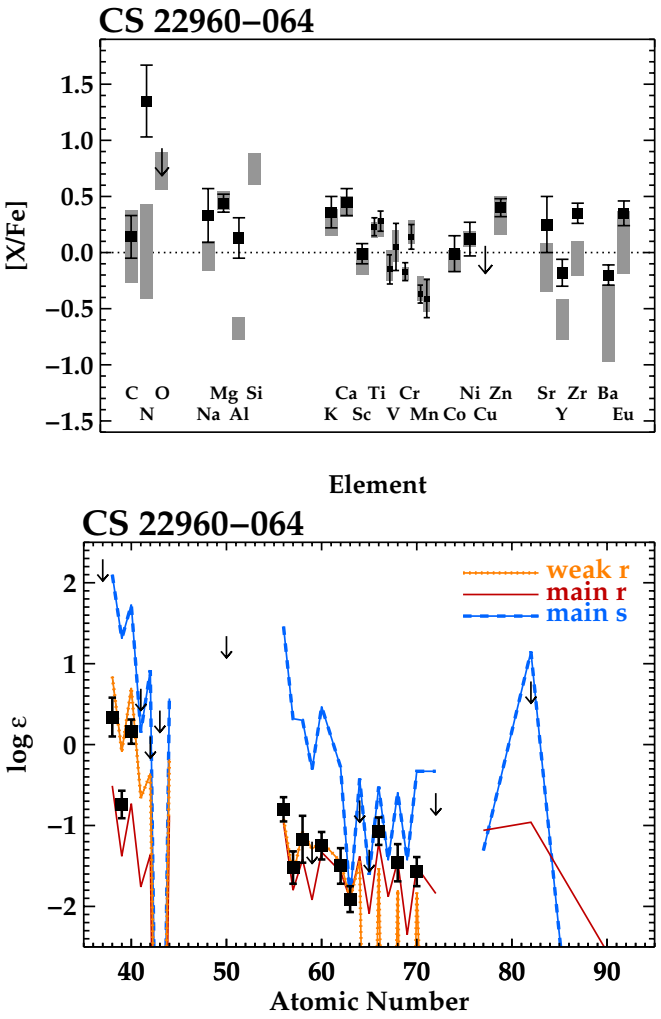

Figure 19. Top: comparison of abundances in CS 22960–064 with the average abundances of 18 other stars with $T_{\rm eff}$ within ±200 K and [Fe/H] within ±0.3 dex of CS 22960–064. Bottom: the heavy element distribution in CS 22960–064. Each of the three curves has been renormalized to the europium abundance in CS 22960–064. Symbols in both panels are the same as in Figure 9.

(A color version of this figure is available in the online journal.)

5. DISCUSSION

Elements produced by neutron-capture reactions are found in all stars in our sample. These heavy elements could not have been manufactured in situ by the low-mass stars where they are found today. At least some of these heavy elements appear to have been produced via *r*-process nucleosynthesis. Our sample is not constructed to represent an unbiased sample of stars, so distributions of, e.g., [Ba/Sr] ratios should not be used as diagnostic tools to attempt to discern the origin of these heavy elements.

Limited samples of stars in a few Local Group ultra-faint dwarf galaxies suggest these systems may have been enriched by metals from a single supernova (Simon et al. 2010; Frebel & Bromm 2012). Previous work has shown that strontium and barium are detected in nearly all low-metallicity stars and at least some stars in all galaxies examined in sufficient detail (Roederer et al. 2010; Roederer 2013). In the Roederer et al. (2014) abundance survey of low-metallicity stars, strontium and barium are detected[5] in all 107 stars with [Fe/H] < -2.0 and $T_{\rm eff} < 5400$ K (i.e., the stars with the lowest continuous opacity and thus strongest lines for a given composition).

Sub-solar [Ba/Sr] ratios are not unique to *r*-process nucleosynthesis predictions. The presence of one star with at least a partial contribution from *s*-process nucleosynthesis, CS 22878–101, serves as a reminder that some *s*-process signatures may offer an alternative, if perhaps less frequent, explanation. Models of the *s*-process operating in low-metallicity rapidly rotating massive stars, affectionately known as spinstars, also predict a range of sub-solar [Ba/Sr] ratios (Frischknecht et al. 2012; Cescutti et al. 2013). The enhanced production of primary ^{22}Ne in the fast rotating models provides a neutron source that enables *s*-process nucleosynthesis. These models require seed nuclei from the iron group, so this non-standard *s*-process nucleosynthesis still operates as a

[5] Roederer et al. (2014) did not detect barium in CS 22968–014, but François et al. (2007) did.

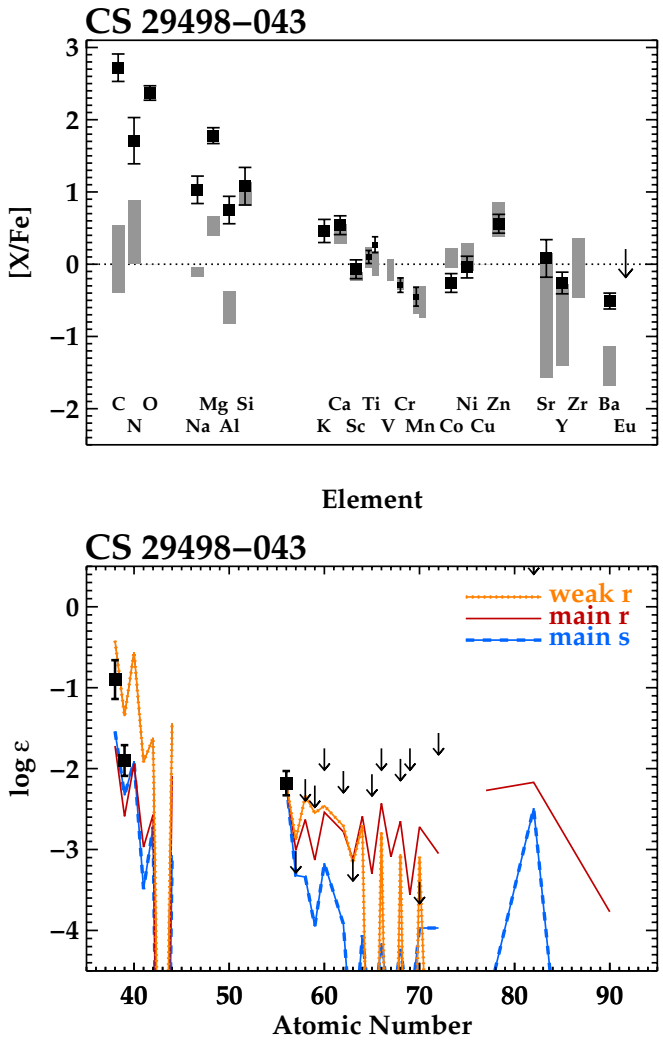

Figure 20. Top: comparison of abundances in CS 29498–043 with the average abundances of six other stars with $T_{\rm eff}$ within ±200 K and [Fe/H] within ±0.3 dex of CS 29498–043. Bottom: the heavy element distribution in CS 29498–043. Each of the three curves has been renormalized to the barium abundance in CS 29498–043. Symbols in both panels are the same as in Figure 9.
(A color version of this figure is available in the online journal.)

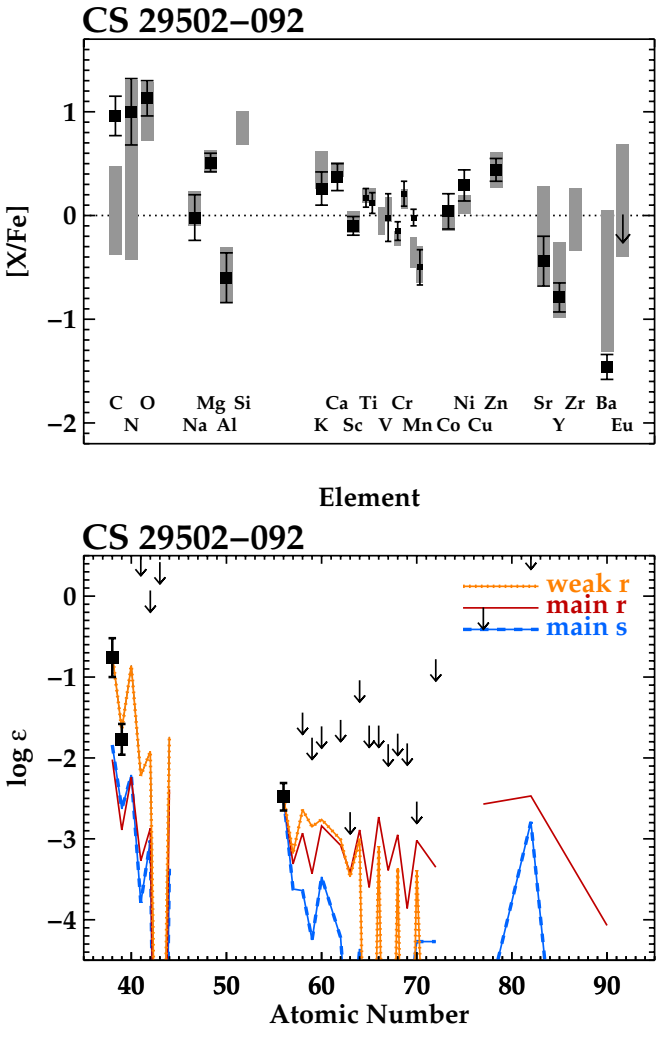

Figure 21. Top: comparison of abundances in CS 29502–092 with the average abundances of 29 other stars with $T_{\rm eff}$ within ±200 K and [Fe/H] within ±0.3 dex of CS 29502–092. Bottom: the heavy element distribution in CS 29502–092. Each of the three curves has been renormalized to the barium abundance in CS 29502–092. Symbols in both panels are the same as in Figure 9.
(A color version of this figure is available in the online journal.)

secondary process (Frischknecht et al.). Spinstars and other sources of *s*-process material at extremely low metallicities may be considered possible sources of the neutron-capture elements in our sample only if their progenitors were not zero-metallicity stars.

Spinstars can be excluded outright in the four stars where the rare earth elements reveal a clear *r*-process origin. If, however, models of these massive stars are shown to host some form of *r*-process nucleosynthesis during the subsequent supernova explosions, this would revive their candidacy for having enriched the gas from which the stars in our sample formed.

Models of pair-instability supernovae predict no neutron-capture element production (e.g., Heger & Woosley 2002). If so, then the results presented here and the lack of environments devoid of neutron-capture elements suggest that pair-instability supernovae were not frequent contributors to the metals in the earliest generations of stars. We are not the first to point out this situation (e.g., Umeda & Nomoto 2002), but our efforts to improve the observational data on neutron-capture elements in low-metallicity stars reaffirm earlier conclusions based on other observational signatures.

Heger & Woosley (2002) emphasize (in the context of pair-instability supernovae) that the simplest explanation for the presence of neutron-capture elements is an additional contribution from normal supernovae. We encourage investigators computing supernova yields to extend their reaction networks to include nuclei produced by neutron-capture nucleosynthesis. This, of course, is challenging because of the number of nuclei involved and the availability of relevant nuclear data for radioactive nuclei far from stability. At the very least, we recommend that such analyses report whether the physical conditions present are capable of supporting neutron-capture nucleosynthesis. These comparisons are essential to determine whether a single supernova can account for all metals observed in each star or whether multiple supernovae are required.

6. SUMMARY

We have studied the heavy element abundance patterns found in 16 stars with sub-solar neutron-capture element abundances and enhanced in carbon or nitrogen (specifically, [Ba/Fe] < 0.0 and either [C/Fe] or [N/Fe] > +1.0). These stars span

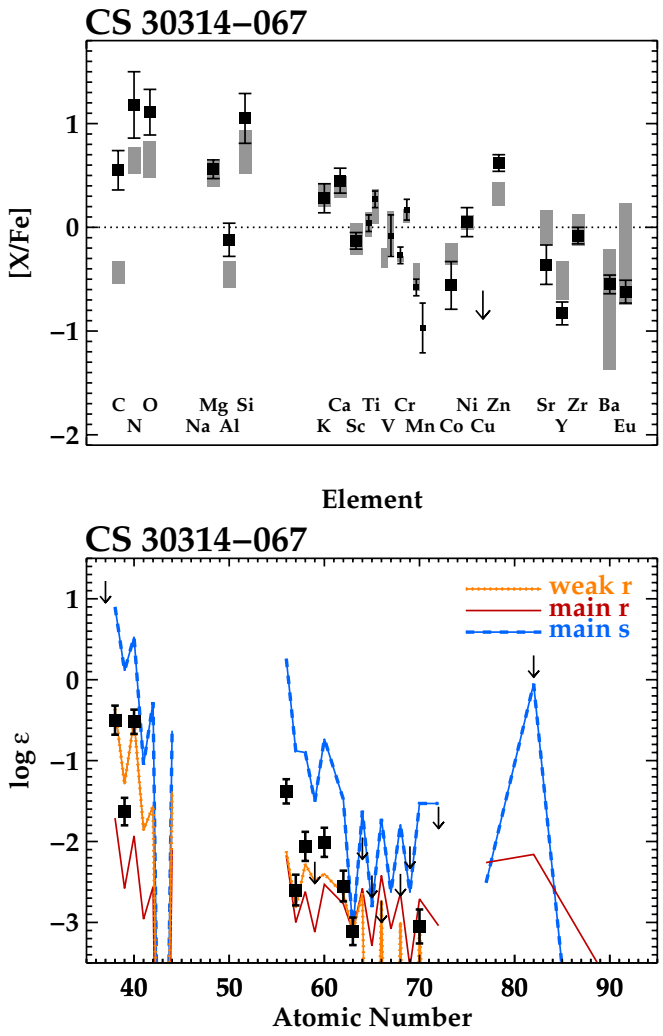

Figure 22. Top: comparison of abundances in CS 30314–067 with the average abundances of six other stars with $T_{\rm eff}$ within ±200 K and [Fe/H] within ±0.3 dex of CS 30314–067. Bottom: the heavy element distribution in CS 30314–067. Each of the three curves has been renormalized to the europium abundance in CS 30314–067. Symbols in both panels are the same as in Figure 9.

(A color version of this figure is available in the online journal.)

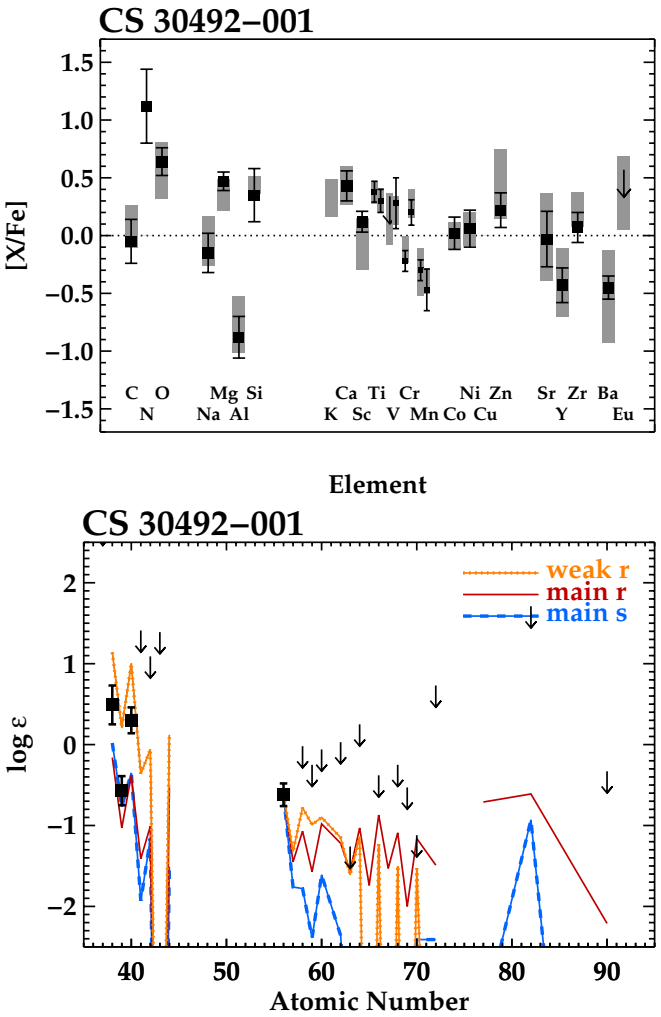

Figure 23. Top: comparison of abundances in CS 30492–001 with the average abundances of 19 other stars with $T_{\rm eff}$ within ±200 K and [Fe/H] within ±0.3 dex of CS 30492–001. Bottom: the heavy element distribution in CS 30492–001. Each of the three curves has been renormalized to the barium abundance in CS 30492–001. Symbols in both panels are the same as in Figure 9.

(A color version of this figure is available in the online journal.)

a metallicity range from $-4.3 < [{\rm Fe/H}] < -2.3$ with a median [Fe/H] of −3.2. The abundance patterns of the lighter elements suggest that this sample could represent the higher-metallicity analogs of the three known CEMP stars with $[{\rm Fe/H}] < -4.5$. High quality optical spectra collected with the MIKE Spectrograph on the Magellan Telescopes and the Tull Spectrograph on the Smith Telescope have allowed us to detect weak absorption lines and derive detailed abundance patterns of elements beyond the iron group.

Strontium is detected in all 16 stars, and barium is detected in 15 of 16 stars. These elements lie at (beyond) the first and second *s*- (*r*-) process peaks, respectively, indicating the operation of at least one form of neutron-capture nucleosynthesis in the progenitors that enriched the stars in our sample. We also detect rare earth elements in five stars, and we use these abundance patterns to characterize the nature of the neutron-capture nucleosynthesis in each of those cases. Some form of *r*-process nucleosynthesis is responsible for the abundance patterns in four of them, and some *s*-process material may be present in another. The [Ba/Sr] ratios in the remaining 11 stars are similar to or lower than the [Ba/Sr] ratios in these 5 stars.

These heavy elements could not have been manufactured in situ by the low-mass stars where they are found today. Rapidly rotating massive stars (spinstars) may be able to account for the heavy elements in the stars without clear evidence of *r*-process nucleosynthesis only if their progenitors were not zero-metallicity stars. The presence of neutron-capture elements in the CEMP-no and NEMP-no stars also suggests that pair instability supernovae were not frequent contributors to the metals in the earliest generations of stars.

Observations do not indicate that all first generation stars must have produced large amounts of carbon and oxygen in their ejecta, but perhaps only those that did enabled low-mass stars that are poor in iron to form. Our conclusions regarding the possibility of neutron-capture production are only applicable, of course, to that set of progenitors. Low-mass stars formed via other cooling modes, like thermal emission by dust grains, provide a glimpse into alternate enrichment environments. The neutron-capture abundance patterns discussed here are not unique to the CEMP-no and NEMP-no classes of stars. Even if the stars considered by us were not formed from the yields of only one supernova each, the nearly ubiquitous presence of

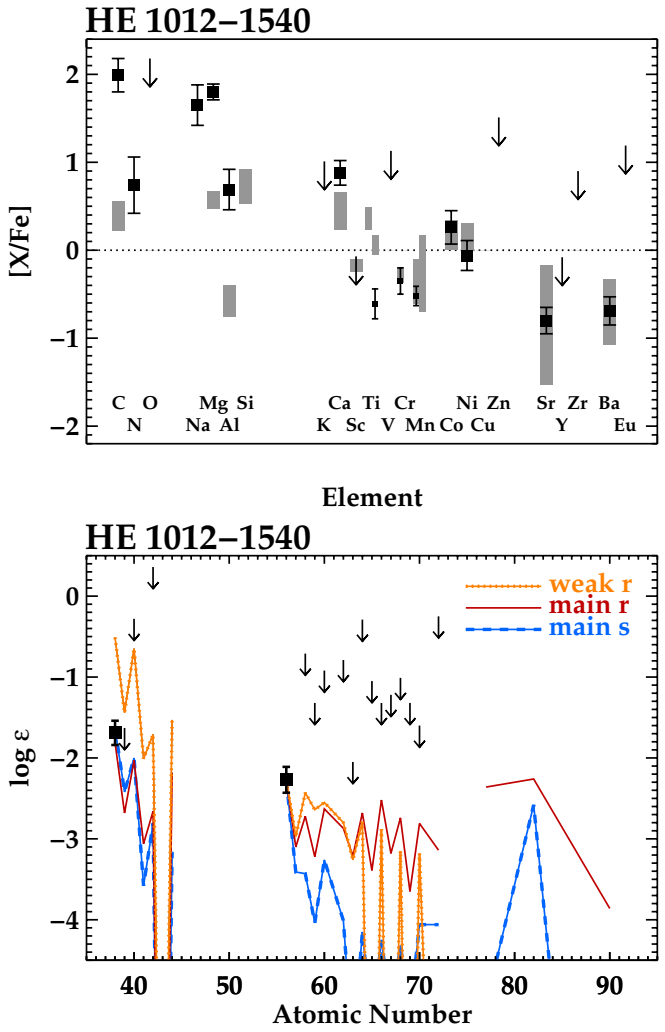

Figure 24. Top: comparison of abundances in HE 1012−1540 with the average abundances of five other stars with $T_{\rm eff}$ within ±200 K and [Fe/H] within ±0.5 dex of HE 1012−1540. Bottom: the heavy element distribution in HE 1012−1540. Each of the three curves has been renormalized to the barium abundance in HE 1012−1540. Symbols in both panels are the same as in Figure 9.

(A color version of this figure is available in the online journal.)

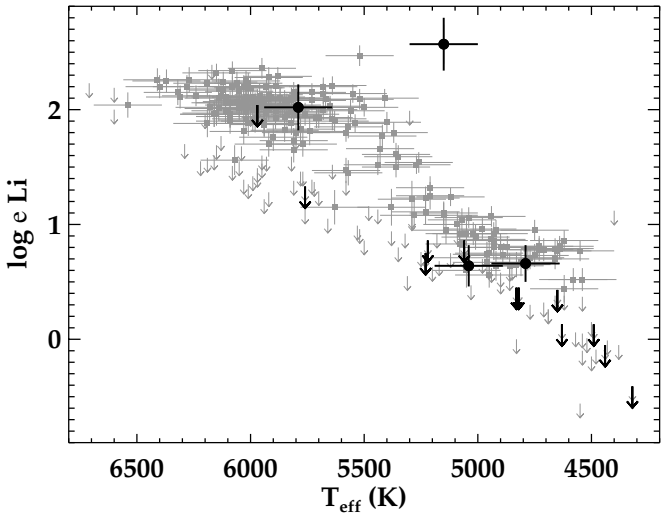

Figure 25. log ϵ lithium abundances as a function of $T_{\rm eff}$. Large black symbols mark the 16 stars in our sample. Small gray symbols mark stars from the main sequence turnoff to the tip of the red giant branch from the full sample of Roederer et al. (2014). Filled symbols represent detections, and arrows indicate upper limits.

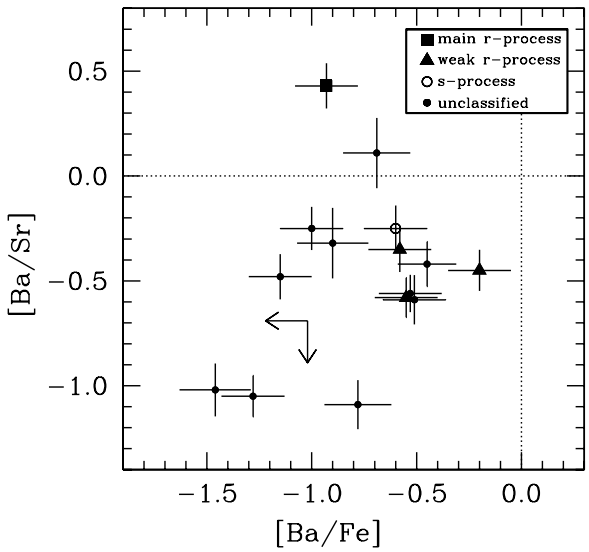

Figure 26. [Ba/Sr] ratios as a function of [Ba/Fe] for our sample. The large square indicates one star likely to have been enriched with products of the main component of the *r*-process (CS 22891–200), the large triangles indicate stars likely to have been enriched with products of the weak component of the *r*-process (CS 22877–001, CS 22960–064, CS 30314–067), the open circle indicates one star likely to have been partly enriched with products of the *s*-process (CS 22878–101), and the small filled circles indicate all other stars in our sample. The dotted lines mark the solar ratios.

strontium and barium in these and other low-metallicity stars is a tantalizing hint that at least one neutron-capture process may have operated frequently in the earliest stellar generations.

If enhanced levels of carbon through silicon (relative to iron) are signatures of nucleosynthesis in prior generations of zero-metallicity stars, and if no other prior generations of stars contributed to the metals, then our results indicate that zero-metallicity stars were also responsible for production of elements beyond the iron group. The early onset of *r*-process nucleosynthesis has long been established (e.g., Truran 1981). Our results offer new evidence in support of Truran's assertion that "a single prior generation of stars can have been responsible for the abundances observed in the most metal-deficient stars in our galaxy" (p. 393).

I.U.R. thanks T. Beers for helpful discussions throughout the course of this study and M. Spite for reaffirming europium upper limits in her data. We thank the referee for a thoughtful and helpful report. This research has made use of NASA's Astrophysics Data System Bibliographic Services, the arXiv preprint server operated by Cornell University, the SIMBAD and VizieR databases hosted by the Strasbourg Astronomical Data Center, and the Atomic Spectra Database hosted by the National Institute of Standards and Technology. IRAF is distributed by the National Optical Astronomy Observatories, which are operated by the Association of Universities for Research in Astronomy, Inc., under cooperative agreement with the National Science Foundation. I.U.R. thanks the Carnegie Institution for Science for support through the Barbara McClintock Fellowship. C.S. is supported by the U.S. National Science Foundation (grant AST 12-11585).

Facilities: Magellan:Baade (MIKE), Magellan:Clay (MIKE), Smith (Tull)

REFERENCES

Aoki, W., Beers, T. C., Christlieb, N., et al. 2007, ApJ, 655, 492
Aoki, W., Frebel, A., Christlieb, N., et al. 2006, ApJ, 639, 897
Aoki, W., Norris, J. E., Ryan, S. G., Beers, T. C., & Ando, H. 2002a, ApJ, 567, 1166
Aoki, W., Norris, J. E., Ryan, S. G., Beers, T. C., & Ando, H. 2002b, ApJL, 576, L141
Aoki, W., Norris, J. E., Ryan, S. G., et al. 2004, ApJ, 608, 971
Aoki, W., Ryan, S. G., Norris, J. E., et al. 2002c, ApJ, 580, 1149
Asplund, M., Grevesse, N., Sauval, A. J., & Scott, P. 2009, ARA&A, 47, 481
Barklem, P. S., & Aspelund-Johansson, J. 2005, A&A, 435, 373
Barklem, P. S., Piskunov, N., & O'Mara, B. J. 2000, A&AS, 142, 467
Becker, G. D., Sargent, W. L. W., Rauch, M., & Carswell, R. F. 2012, ApJ, 744, 91
Beers, T. C., & Christlieb, N. 2005, ARA&A, 43, 531
Bernstein, R., Shectman, S. A., Gunnels, S. M., Mochnacki, S., & Athey, A. E. 2003, Proc. SPIE, 4841, 1694
Bessell, M. S., Christlieb, N., & Gustafsson, B. 2004, ApJL, 612, L61
Bisterzo, S., Gallino, R., Straniero, O., Cristallo, S., & Käppeler, F. 2011, MNRAS, 418, 284
Bonifacio, P., Molaro, P., Beers, T. C., & Vladilo, G. 1998, A&A, 332, 672
Bonifacio, P., Spite, M., Cayrel, R., et al. 2009, A&A, 501, 519
Brown, J. A., Sneden, C., Lambert, D. L., & Dutchover, E., Jr. 1989, ApJS, 71, 293
Caffau, E., Bonifacio, P., François, P., et al. 2012, A&A, 542, A51
Carney, B. W., Latham, D. W., Stefanik, R. P., Laird, J. B., & Morse, J. A. 2003, AJ, 125, 293
Carollo, D., Beers, T. C., Bovy, J., et al. 2012, ApJ, 744, 195
Carretta, E., Gratton, R., Cohen, J. G., Beers, T. C., & Christlieb, N. 2002, AJ, 124, 481
Cayrel, R., Depagne, E., Spite, M., et al. 2004, A&A, 416, 1117
Cescutti, G., Chiappini, C., Hirschi, R., Meynet, G., & Frischknecht, U. 2013, A&A, 553, A51
Christlieb, N., Bessell, M. S., Beers, T. C., et al. 2002, Natur, 419, 904
Christlieb, N., Gustafsson, B., Korn, A. J., et al. 2004, ApJ, 603, 708
Cohen, J. G., Christlieb, N., Beers, T. C., Gratton, R., & Carretta, E. 2002, AJ, 124, 470
Cohen, J. G., Christlieb, N., McWilliam, A., et al. 2008, ApJ, 672, 320
Cohen, J. G., Christlieb, N., Thompson, I. B., et al. 2013, ApJ, 778, 56
Cohen, J. G., McWilliam, A., Shectman, S., et al. 2006, AJ, 132, 137
Cooke, R., Pettini, M., Steidel, C. C., Rudie, G. C., & Jorgenson, R. A. 2011a, MNRAS, 412, 1047
Cooke, R., Pettini, M., Steidel, C. C., Rudie, G. C., & Nissen, P. E. 2011b, MNRAS, 417, 1534
Demarque, P., Woo, J.-H., Kim, Y.-C., & Yi, S. K. 2004, ApJS, 155, 667
Depagne, E., Hill, V., Spite, M., et al. 2002, A&A, 390, 187
Fabbian, D., Asplund, M., Barklem, P. S., Carlsson, M., & Kiselman, D. 2009, A&A, 500, 1221
François, P., Depagne, E., Hill, V., et al. 2007, A&A, 476, 935
Frebel, A., Aoki, W., Christlieb, N., et al. 2005, Natur, 434, 871
Frebel, A., & Bromm, V. 2012, ApJ, 759, 115
Frebel, A., Christlieb, N., Norris, J. E., Aoki, W., & Asplund, M. 2006, ApJL, 638, L17
Frebel, A., Collet, R., Eriksson, K., Christlieb, N., & Aoki, W. 2008, ApJ, 684, 588
Frebel, A., Simon, J. D., Geha, M., & Willman, B. 2010, ApJ, 708, 560
Frischknecht, U., Hirschi, R., & Thielemann, F.-K. 2012, A&A, 538, L2
Fryer, C. L., Woosley, S. E., & Heger, A. 2001, ApJ, 550, 372
Fulbright, J. P. 2002, AJ, 123, 404
Gallino, R., Arlandini, C., Busso, M., et al. 1998, ApJ, 497, 388
Gilmore, G., Norris, J. E., Monaco, L., et al. 2013, ApJ, 763, 61
Giridhar, S., Lambert, D. L., Gonzalez, G., & Pandey, G. 2001, PASP, 113, 519
Gratton, R. G., Carretta, E., Desidera, S., et al. 2003, A&A, 406, 131
Gustafsson, B., Edvardsson, B., Eriksson, K., et al. 2008, A&A, 486, 951
Heger, A., & Woosley, S. E. 2002, ApJ, 567, 532
Hollek, J. K., Frebel, A., Roederer, I. U., et al. 2011, ApJ, 742, 54
Honda, S., Aoki, W., Ando, H., et al. 2004, ApJS, 152, 113
Honda, S., Aoki, W., Ishimaru, Y., Wanajo, S., & Ryan, S. G. 2006, ApJ, 643, 1180
Ishigaki, M., Chiba, M., & Aoki, W. 2010, PASJ, 62, 143
Ishigaki, M. N., Aoki, W., & Chiba, M. 2013, ApJ, 771, 67
Ito, H., Aoki, W., Beers, T. C., Tominaga, N., et al. 2013, ApJ, 773, 33
Ito, H., Aoki, W., Honda, S., & Beers, T. C. 2009, ApJL, 698, L37
Johnson, J. A. 2002, ApJS, 139, 219
Johnson, J. A., Herwig, F., Beers, T. C., & Christlieb, N. 2007, ApJ, 658, 1203
Kelson, D. D. 2003, PASP, 115, 688
Kirby, E. N., Fu, X., Guhathakurta, P., & Deng, L. 2012, ApJL, 752, L16
Koch, A., Feltzing, S., Adén, D., & Matteucci, F. 2013, A&A, 554, A5
Kurucz, R. L., & Bell, B. 1995, Kurucz CD-ROM (Cambridge, MA: Smithsonian Astrophysical Observatory)
Lai, D. K., Bolte, M., Johnson, J. A., & Lucatello, S. 2004, AJ, 128, 2402
Lai, D. K., Bolte, M., Johnson, J. A., et al. 2008, ApJ, 681, 1524
Lai, D. K., Lee, Y. S., Bolte, M., et al. 2011, ApJ, 738, 51
Lambert, D. L., & Sawyer, S. R. 1984, ApJ, 283, 192
Lebzelter, T., Uttenthaler, S., Busso, M., Schultheis, M., & Aringer, B. 2012, A&A, 538, A36
Lind, K., Asplund, M., & Barklem, P. S. 2009, A&A, 503, 541
Lind, K., Asplund, M., Barklem, P. S., & Belyaev, A. K. 2011, A&A, 528, A103
Martell, S. L., & Shetrone, M. D. 2013, MNRAS, 430, 611
McWilliam, A., Preston, G. W., Sneden, C., & Searle, L. 1995a, AJ, 109, 2757
McWilliam, A., Preston, G. W., Sneden, C., & Shectman, S. 1995b, AJ, 109, 2736
Meynet, G., Ekström, S., & Maeder, A. 2006, A&A, 447, 623
Meynet, G., Hirschi, R., Ekstrom, S., et al. 2010, A&A, 521, A30
Nissen, P. E., & Schuster, W. J. 2010, A&A, 511, L10
Norris, J. E., Christlieb, N., Bessell, M. S., et al. 2012, ApJ, 753, 150
Norris, J. E., Christlieb, N., Korn, A. J., et al. 2007, ApJ, 670, 774
Norris, J. E., Gilmore, G., Wyse, R. F. G., Yong, D., & Frebel, A. 2010a, ApJL, 722, L104
Norris, J. E., Ryan, S. G., & Beers, T. C. 1997, ApJL, 489, L169
Norris, J. E., Ryan, S. G., & Beers, T. C. 2001, ApJ, 561, 1034
Norris, J. E., Ryan, S. G., Beers, T. C., Aoki, W., & Ando, H. 2002, ApJL, 569, L107
Norris, J. E., Yong, D., Bessell, M. S., et al. 2013, ApJ, 762, 28
Norris, J. E., Yong, D., Gilmore, G., & Wyse, R. F. G. 2010b, ApJ, 711, 350
Pilachowski, C. A., Sneden, C., Kraft, R. P., Harmer, D., & Willmarth, D. 2000, AJ, 119, 2895
Piskunov, N. E., & Valenti, J. A. 2002, A&A, 385, 1095
Preston, G. W., & Sneden, C. 2001, AJ, 122, 1545
Primas, F., Molaro, P., & Castelli, F. 1994, A&A, 290, 885
Roederer, I. U. 2009, AJ, 137, 272
Roederer, I. U. 2013, AJ, 145, 26
Roederer, I. U., Cowan, J. J., Karakas, A. I., et al. 2010, ApJ, 724, 975
Roederer, I. U., Frebel, A., Shetrone, M. D., et al. 2008, ApJ, 679, 1549
Roederer, I. U., Kratz, K.-L., Frebel, A., et al. 2009, ApJ, 698, 1963
Roederer, I. U., Lawler, J. E., Sobeck, J. S., et al. 2012, ApJS, 203, 27
Roederer, I. U., Preston, G. W., Thompson, I. B., et al. 2014, AJ, submitted
Ruchti, G. R., Fulbright, J. P., Wyse, R. F. G., et al. 2011a, ApJ, 737, 9
Ruchti, G. R., Fulbright, J. P., Wyse, R. F. G., et al. 2011b, ApJ, 743, 107
Ryan, S. G., Aoki, W., Norris, J. E., & Beers, T. C. 2005, ApJ, 635, 349
Simon, J. D., Frebel, A., McWilliam, A., Kirby, E. N., & Thompson, I. B. 2010, ApJ, 716, 446
Sivarani, T., Beers, T. C., Bonifacio, P., et al. 2006, A&A, 459, 125
Sneden, C. A. 1973, PhD thesis, Univ. of Texas at Austin
Sneden, C., Cowan, J. J., & Gallino, R. 2008, ARA&A, 46, 241
Sneden, C., Cowan, J. J., Lawler, J. E., et al. 2003, ApJ, 591, 936
Sneden, C., Lawler, J. E., Cowan, J. J., Ivans, I. I., & Den Hartog, E. A. 2009, ApJS, 182, 80
Sobeck, J. S., Kraft, R. P., Sneden, C., et al. 2011, AJ, 141, 175
Spite, M., Cayrel, R., Plez, B., et al. 2005, A&A, 430, 655
Stephens, A., & Boesgaard, A. M. 2002, AJ, 123, 1647
Takeda, Y., Zhao, G., Chen, Y.-Q., Qiu, H.-M., & Takada-Hidai, M. 2002, PASJ, 54, 275
Thorburn, J. A. 1994, ApJ, 421, 318
Tominaga, N., Iwamoto, N., & Nomoto, K. 2013, ApJ, in press (arXiv:1309.6734)
Tominaga, N., Maeda, K., Umeda, H., et al. 2007, ApJL, 657, L77
Truran, J. W. 1981, A&A, 97, 391
Tsangarides, S., Ryan, S. G., & Beers, T. C. 2004, MmSAI, 75, 772
Tull, R. G., MacQueen, P. J., Sneden, C., & Lambert, D. L. 1995, PASP, 107, 251
Tumlinson, J. 2006, ApJ, 641, 1
Umeda, H., & Nomoto, K. 2002, ApJ, 565, 385
Umeda, H., & Nomoto, K. 2003, Natur, 422, 871
Umeda, H., & Nomoto, K. 2005, ApJ, 619, 427
Unsöld, A. 1955, Physik der Sternatmosphären (Berlin: Springer), 332
Yong, D., Norris, J. E., Bessell, M. S., et al. 2013, ApJ, 762, 26